Physics – Uspekhi **64** (12) 1238 – 1260 (2021)

REVIEWS OF TOPICAL PROBLEMS

PACS numbers: 14.60.Pq, 14.60.St, **23.40. – s**

50th ANNIVERSARY OF THE INSTITUTE FOR NUCLEAR RESEARCH, RAS

Neutrino masses and interactions and neutrino experiments in the laboratory

F Šimkovic

DOI: https://doi.org/10.3367/UFNe.2021.08.039036

Contents

Abstract. The atomic nucleus offers a unique opportunity to study fundamental properties and interactions of neutrinos. The main subjects of interest are the nature of neutrinos (Dirac or Majorana), mass hierarchy, the absolute scale of neutrino masses, and possible additional sterile neutrinos. In this review, recent progress in the field of laboratory measurements of fundamental properties of neutrinos is briefly presented.

Keywords: lepton number violation, Dirac and Majorana neutrinos, neutrino masses and mixing, neutrino oscillations, tritium beta decay, two-neutrino and neutrinoless double beta decay, nuclear matrix elements, axial-vector coupling constant

1. Introduction

Neutrinos are fundamental particles that were first formed in the first second of the early Universe and are continually being produced in astrophysical processes across the cosmic space, e.g., in the nuclear reactions of stars, like our Sun, supernova explosions, cosmic particle accelerators, etc. They are also produced by cosmic-ray interactions with Earth's atmosphere, from natural radioactive decays inside Earth, in an artificial way at nuclear power plants, and with help of particle accelerators. Neutrinos are likely the most abundant particles in the Universe and may be more common than photons, representing a new 'window' on the Universe, spanning a large range of energy.

The neutrino was postulated by Wolfgang Pauli to preserve the principles of energy and angular momentum conservation in nuclear β-decay already nine decades ago. We know now that there are not just one but three different kinds (flavors) of neutrinos: electrons, muons and tau neutrinos (ν_e, ν_μ, and ν_τ), entering the weak-interaction of the Standard Model (SM) of particle physics. The revolutionary discovery of neutrino oscillations at the end of the 20th century [1, 2] showed that neutrinos have mass, and that neutrinos with well-defined flavors are a mixture (linear superpositions) of neutrinos with well-defined mass (the pre-condition for oscillation is termed 'mixing'). It has been noted that neutrino masses contradict the SM, where neutrinos are strictly massless.

The tiny masses of neutrinos and the transformations of one neutrino type to another have even revealed physics beyond the Standard Model of particle physics. Studying and understanding neutrino mass and oscillation provide a unique view into how forces and particles are unified. The observed structure of neutrino mixing, namely the existence

F Šimkovic [1, 2, 3]
[1] Department of Nuclear Physics and Biophysics, Comenius University, Mlynská dolina F1, SK–842 15 Bratislava, Slovakia
[2] Joint Institute for Nuclear Research, Bogoliubov Laboratory of Theoretical Physics, ul. Joliot-Curie 6, 141980 Dubna, Moscow region, Russian Federation
[3] Czech Technical University in Prague, Jugoslávských partyzánů 1580/3, CZ-12800 Prague, Czech Republic
E-mail: fedor.simkovic@fmph.uniba.sk

Received 11 June 2021, revised 3 August 2021
Uspekhi Fizicheskikh Nauk **191** (12) 1307 – 1332 (2021)

of two large mixing angles, is very different from the quark sector. This fact may be understood as an indication of physics beyond the SM, since neutrinos may obtain their mass in a different way than other fundamental fermions.

The discovery of neutrino oscillations has created new opportunities to use neutrinos to advance our knowledge of the Universe and the laws that govern it. Neutrinos are the only known weakly interacting massive particles, and thus they are the only known component of dark matter. It is intriguing that the mass scale of neutrinos and the energy scale of dark energy are approximately the same. A possible CP violation in the neutrino sector can explain the baryon asymmetry of the Universe, i.e., why we are made out of matter and not antimatter. Because neutrinos are so common, their mass, which remains unknown, is thought to have an effect on the gravity of the Universe.

Neutrinos remain the most mysterious of the fundamental fermions, and we still do not know the answers to several undeniably fundamental questions. The subjects of main interest are the absolute neutrino mass scale, the neutrino mass hierarchy, the nature of neutrinos (Dirac or Majorana), the CP properties of neutrinos, and the possible existence of additional sterile neutrinos. An atomic nucleus is a laboratory to study fundamental properties and interactions of neutrinos. In this review, recent progress in the field of laboratory measurements of neutrino masses and interactions is briefly presented.

2. Neutrino masses and mixing

2.1 Generation of neutrino masses

From the discovery of neutrino oscillations, the measurement of neutrino masses in tritium laboratory experiments, and cosmological data, it follows that neutrino masses are many orders of magnitude smaller than the masses of other Standard Model fermions. The smallness of the neutrino mass is one of the major unresolved problems of particle physics theory. It seems to be very plausible that neutrino masses and those of charged leptons and quarks are of different origins.

A favorable scenario is that this phenomenon is related to a broken symmetry of the total lepton number at some high-energy scale Λ. Then, on the electroweak scale, the $\Delta L = 2$ effective Weinberg operator of dimension-5 appears [3]:

$$\mathcal{O}_{\rm W} = \frac{f_{\alpha\beta}}{\Lambda}\,\overline{L_\alpha^C} H L_\beta H\,, \tag{1}$$

where H is the Higgs doublet of the SM taken to have a hypercharge opposite to that of the lepton doublets L_α, where $\alpha = 1, 2, 3$ is the family index. This operator is nonrenormalizable and unique as only Standard Model scalar fields are considered. After electroweak symmetry breaking (EWSB), $\sqrt{2}\langle H^0\rangle = v = 246$ GeV, in the three tree-level realizations of the effective operator in Eqn (1), one ends up with the Majorana neutrino mass matrix of active neutrinos

$$m_{\alpha\beta} = -f_{\alpha\beta}\, v\, \frac{v}{\Lambda}\,. \tag{2}$$

For a generic case with $f \sim 1$ and for naturally small neutrino masses at a sub-eV scale, the estimate $\Lambda \sim 10^{14} - 10^{15}$ GeV is made.

There are many particle physics models which lead to the dimension-5 Weinberg effective operator once heavy particle fields are integrated out. The Majorana mass term is generated through new messenger particles, where Λ points to the scale of their masses which, being very heavy, have no phenomenological manifestation. The tree-level exchange by heavy singlet fermions/neutrinos induces small neutrino masses through what is now generically called the type-I seesaw mechanism [4–7]. The heavy messengers can also be extra scalar Higgs bosons (such as scalar triplets) and triplet fermions in the type-II [8–12] and type-III [13–16] seesaw realizations, respectively. In spite of the fact that all these models explain the smallness of neutrino masses, the absolute values of masses can not be predicted, as many unknown parameters are involved.

The new physics scale can be reduced to the TeV ballpark accessible at the Large Hadron Collider (LHC) in models which relax the above standard seesaw limitation on the lepton-number violation (LNV) scale by introducing an additional suppression mechanism for neutrino masses. It might happen, e.g., if the neutrino masses are generated radiatively (see, e.g., Refs [17–24]) or forbidden or suppressed at dimension-5, but appears from effective operators of higher dimensions [25–27].

The subject of interest is the class of the SM gauge-invariant effective operators of dimension-7 [28]:

$$\begin{aligned} \mathcal{O}_7^{\rm u} &= \frac{g^{\rm u}_{\alpha\beta}}{\Lambda^3}\,\overline{L_\alpha^C} L_\beta\, H\, \bar{Q} u_{\rm R}\,, \\ \mathcal{O}_7^{\rm d} &= \frac{g^{\rm d}_{\alpha\beta}}{\Lambda^3}\,\overline{L_\alpha^C} L_\beta\, H\, \bar{d}_{\rm R} Q\,. \end{aligned} \tag{3}$$

Here, all the possible $\mathrm{SU(2)_L}$ contractions are assumed. The operators (3) were previously studied in the literature as a source of $\Delta L = 2$ interactions able to induce $0\nu\beta\beta$-decay with no explicit dependence on the Majorana neutrino mass [29–33]. On the other hand, it was observed in Ref. [34] that this operator contributes to the Majorana-neutrino mass matrix due to spontaneous breaking of chiral symmetry (SBCS) via the light-quark condensate $\langle\overline{\rm q}{\rm q}\rangle = -\omega^3 \neq 0$, which sets the SBCS scale, so that after EWSB and SBCS one arrives at the contribution to the Majorana mass matrix of active neutrinos [28]:

$$m^{\nu}_{\alpha\beta} = -g_{\alpha\beta}\, v\, \frac{\langle\overline{\rm q}{\rm q}\rangle}{\Lambda^3} = g_{\alpha\beta}\, v \left(\frac{\omega}{\Lambda}\right)^3\,, \tag{4}$$

with $g_{\alpha\beta} = g^{\rm u}_{\alpha\beta} + g^{\rm d}_{\alpha\beta}$, where $\langle\overline{\rm q}{\rm q}\rangle \equiv \langle\overline{\rm u}{\rm u}\rangle \approx \langle\overline{\rm d}{\rm d}\rangle \approx 2\,\langle\overline{u_{\rm L}}\, u_{\rm R}\rangle \approx 2\,\langle\overline{d_{\rm R}}\, d_{\rm L}\rangle$. This is a kind of seesaw formula relating the smallness of the Majorana masses of neutrinos to the large ratio between the scale Λ of lepton-number violation and the scale of chiral-symmetry breaking $\omega = -\langle\overline{q}q\rangle^{1/3}$. We call relation (4) the quark condensate seesaw (QCSS) formula. Taking

$$\langle\overline{\rm q}{\rm q}\rangle^{1/3} \approx -283\ {\rm MeV}\,, \tag{5}$$

from a renormalized lattice QCD within the $\overline{\rm MS}$ scheme at a fixed scale $\mu = 2$ GeV [35] and $\Lambda \sim$ a few TeV, we get the neutrino mass in the sub-eV ballpark [28].

2.2 Phenomenology of neutrino masses within three-neutrino mixing scheme

The observation of neutrino oscillations established the fact that neutrinos possess small masses and that leptonic flavors

Table 1. Current values from global fits to neutrino oscillation experiments taken from [36]. Recall that mass parameters are defined as $\delta m^2 = m_2^2 - m_1^2$ and $\Delta m^2 = m_3^2 - (m_1^2 + m_2^2)/2$, i.e., $\Delta m^2 > 0$ and $\Delta m^2 < 0$ correspond to the normal hierarchy (NH) and inverted hierarchy (IH) of neutrino masses, respectively. Note that the overall χ^2 difference between NH and IH is insignificant [36].

Parameter	Best fit	1σ	2σ	3σ
Normal hierarchy (NH)				
$\delta m^2/10^{-5}\ \mathrm{eV}^2$	7.34	7.20 – 7.51	7.05 – 7.69	6.92 – 7.90
$\Delta m^2/10^{-3}\ \mathrm{eV}^2$	2.485	2.453 – 2.514	2.419 – 2.547	2.2389 – 2.578
$\sin^2\theta_{12}/10^{-1}$	3.05	2.92 – 3.19	2.78 – 3.32	2.65 – 3.47
$\sin^2\theta_{13}/10^{-2}$	2.22	2.14 – 2.28	2.07 – 2.34	2.01 – 2.41
$\sin^2\theta_{23}/10^{-1}$	5.45	4.98 – 5.65	4.54 – 5.81	4.36 – 5.95
δ/π	1.28	1.10 – 1.66	0.95 – 1.90	$0 - 0.07 \oplus 0.81 - 2.00$
Inverted hierarchy (IH)				
$\delta m^2/10^{-5}\ \mathrm{eV}^2$	7.34	7.20 – 7.51	7.05 – 7.69	6.92 – 7.91
$-\Delta m^2/10^{-3}\ \mathrm{eV}^2$	2.465	2.434 – 2.495	2.404 – 2.526	2.374 – 2.556
$\sin^2\theta_{12}/10^{-1}$	3.03	2.90 – 3.17	2.77 – 3.31	2.64 – 3.45
$\sin^2\theta_{13}/10^{-2}$	2.23	2.17 – 2.30	2.10 – 2.37	2.03 – 2.43
$\sin^2\theta_{23}/10^{-1}$	5.51	$5.17 - 5.67 \oplus 5.31 - 6.10$	4.60 – 5.82	4.39 – 5.96
δ/π	1.52	1.37 – 1.65	1.23 – 1.78	1.09 – 1.90

are not symmetries of Nature. The obtained data are commonly analyzed within a minimal three-neutrino framework, where known flavor states (ν_e, ν_μ, ν_τ) are expressed as quantum superpositions of three massive states ν_i ($i = 1, 2, 3$) with masses m_i. We have

$$|\nu_\alpha\rangle = \sum_{j=1}^{3} U_{\alpha j}^{*} |\nu_j\rangle\,, \qquad \alpha = e, \mu, \tau\,. \tag{6}$$

In the case of Dirac neutrinos, the unitary 3×3 Pontecorvo–Maki–Nakagawa–Sakata (PMNS) neutrino mixing matrix can be parameterized as follows:

$$U = R_{23}\tilde{R}_{13}R_{12}\,, \tag{7}$$

where the matrices R_{ij} are rotations in ij space, i.e.,

$$R_{12} = \begin{pmatrix} c_{12} & s_{12} & 0 \\ -s_{12} & c_{12} & 0 \\ 0 & 0 & 1 \end{pmatrix}, \quad R_{23} = \begin{pmatrix} 1 & 0 & 0 \\ 0 & c_{23} & s_{23} \\ 0 & -s_{23} & c_{23} \end{pmatrix}, \quad \tilde{R}_{13} = \begin{pmatrix} c_{13} & 0 & s_{13}\exp(-i\delta) \\ 0 & 1 & 0 \\ -s_{13}\exp(i\delta) & 0 & c_{13} \end{pmatrix}, \tag{8}$$

where $c_{ij} \equiv \cos\theta_{ij}$, $s_{ij} \equiv \sin\theta_{ij}$, θ_{12}, θ_{13}, and θ_{23} are mixing angles, and δ is the CP phase. If neutrinos are Majorana particles, the matrix U in Eqn (7) is multiplied by a diagonal phase matrix $P = \mathrm{diag}(\exp(i\alpha_1), \exp(i\alpha_2), \exp(i\delta))$, which contains two additional CP phases, α_1 and α_2.

For three neutrino families, neutrino oscillation experiments are sensitive to three mixing angles (θ_{12}, θ_{13}, and θ_{23}), the CP phase δ, and the two independent mass-squared differences, which can be chosen as follows: $\delta m^2 = m_2^2 - m_1^2$ and $\Delta m^2 = m_3^2 - (m_1^2 + m_2^2)/2$ [36]. Two types of neutrino mass spectra are possible:

• Normal Spectrum (NS): $m_1 < m_2 < m_3$: $\Delta m^2 > 0$. In this case,

$$m_2 = \sqrt{\delta m^2 + m_0^2}\,, \quad m_3 = \sqrt{\Delta m^2 + \frac{\delta m^2}{2} + m_0^2}$$

with $m_0 = m_1$.

• Inverted Spectrum (IS), $m_3 < m_1 < m_2$: $\Delta m^2 < 0$. We have

$$m_{1,2} = \sqrt{-\Delta m^2 \mp \frac{\delta m^2}{2} + m_0^2}$$

with $m_0 = m_3$.

Here, $m_0 = m_1(m_3)$ is the lightest neutrino mass. Given the type of neutrino mass spectrum, m_0 fully determines the absolute neutrino mass scale.

The recent updated set of six neutrino oscillation parameters (δm^2, Δm^2, θ_{12}, θ_{13}, θ_{23}, δ) obtained by a global fit of results coming from experiments using neutrinos from solar, atmospheric, accelerator, and reactor sources is presented in Table 1. Currently, this combined analysis allows constraining the previously unknown CP phase δ. Concerning the type of spectrum ($\mathrm{sign}(\Delta m^2)$), there is no indication in favor of normal or inverted mass ordering. However, assuming NS, there is an indication of the other unknown parameter, namely, a preference is found in favor of the first θ_{23} octant ($\theta_{23} < \pi/4$ at $\sim 95\%$ CL).

In order to fix completely the three light neutrino masses, there is just one parameter left to be measured, namely, the absolute neutrino mass scale. No current experiment has sufficient sensitivity to measure it. Terrestrial experiments, such as tritium beta decay, give an upper bound on the absolute neutrino masses. The principle of the experiment is to look for a distortion near the endpoint of the electron spectrum of tritium β-decay. In this direct, model independent, determination of the mass of the neutrino, the meas-

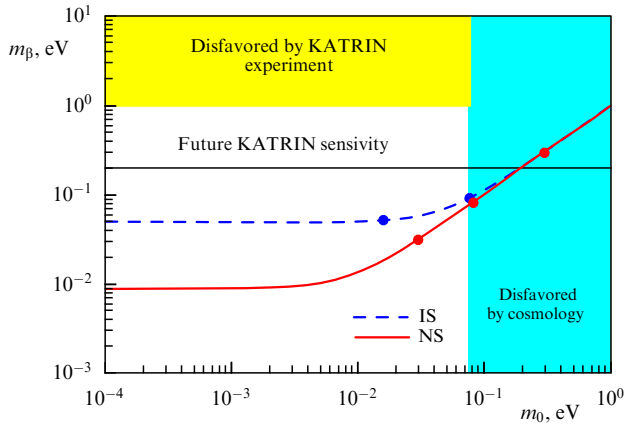

Figure 1. (Color online.) Effective neutrino mass m_β measured in β-decay of tritium as a function of mass of the lowest eigenstate m_0. Results are presented for inverted (IS, $m_0 = m_3$) and normal (NS, $m_0 = m_1$) spectra of neutrino masses. Best fit values of the global fit of neutrino oscillation parameters are considered (see Table 1). Cosmological constraint corresponding to $\Sigma < 0.26$ eV is displayed in turquoise. NS, IS, and the astrophysical limit values of 0.12 eV, 0.26 eV [37], and 0.9 eV [38] are indicated by red and blue dots, respectively.

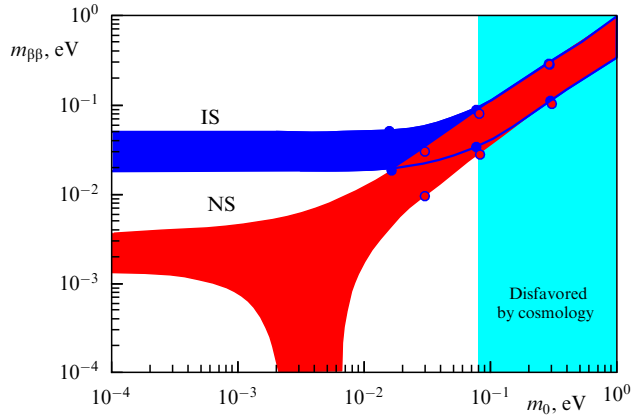

Figure 2. (Color online.) Effective Majorana mass $m_{\beta\beta}$ as a function of mass of the lowest eigenstate m_0. Blue and red bands refer to inverted (IS, $m_0 = m_3$) and normal (NS, $m_0 = m_1$) spectra of neutrino masses, respectively. Best fit values of the global fit of neutrino oscillation parameters are considered (see Table 1). Cosmological constraint corresponding to $\Sigma < 0.26$ eV is displayed in turquoise. Assuming CP conservation, NS, IS, and the astrophysical limit values of 0.12 eV, 0.26 eV [37], and 0.9 eV [38] are indicated by filled circles in red and blue, respectively.

urable quantity is

$$m_\beta = \sqrt{\sum_{k=1}^{3} |U_{ek}|^2 m_k^2}\,. \tag{9}$$

The KArlsruhe TRItium Neutrino (KATRIN) experiment will be able to achieve a sensitivity of $m_\beta < 200$ meV (at 90% CL) [39]. This level represents an order of magnitude improvement over the absolute neutrino mass scale. In Fig. 1, m_β is shown as a function of mass of the lowest eigenstate m_0. It should be noted that, for values of m_0 not excluded by cosmology, m_β depends significantly on the assumption of a normal or inverted neutrino mass spectrum.

If neutrinos are Majorana particles, the effective Majorana mass,

$$m_{\beta\beta} = \left|\sum_{k=1}^{3} U_{ek}^2 m_k\right| = \left|c_{12}^2 c_{13}^2 m_1 + \exp(2i\alpha_{21}) c_{13}^2 s_{12}^2 m_2 + \exp(2i\alpha_{31}) s_{13}^2 m_3\right|, \tag{10}$$

which is measured in 0νββ-decay experiments, can be used to make conclusions about the absolute scale of neutrino masses. In Fig. 2, $m_{\beta\beta}$ is presented as a function of mass of the lowest eigenstate m_0. Results for both inverted and normal spectra of neutrino masses are presented. It can be seen that, in the case of the inverted hierarchy, $m_{\beta\beta}$ is in the range of tens of meV or larger. In the opposite case, a preferable value of $m_{\beta\beta}$ is a few meV, but can be strongly suppressed for m_0 in the range $2 \leqslant m_{\beta\beta} \leqslant 6$ meV.

The quest to determine the neutrino mass scale is complemented by the upper limits from cosmology. Cosmological observations can further constrain neutrino properties by providing a more stringent bound on the sum of the neutrino masses

$$\Sigma = \sum_{k=1}^{3} m_k \tag{11}$$

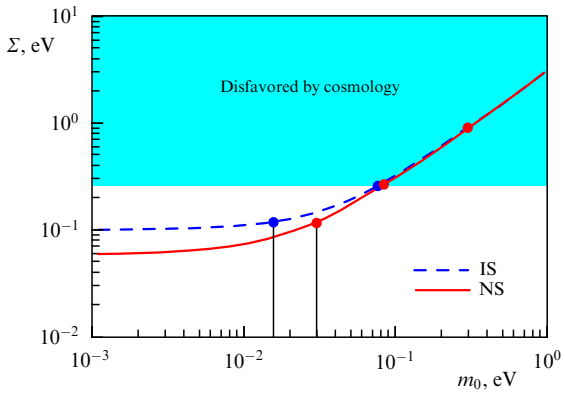

Figure 3. (Color online.) Sum of neutrino masses Σ measured by cosmology as a function of the mass of the lowest eigenstate m_0, Results are presented for inverted (IS, $m_0 = m_3$) and normal (NS, $m_0 = m_1$) spectra of neutrino masses. Best fit values of the global fit of neutrino oscillation parameters are considered (see Table 1). Cosmological constraint corresponding to $\Sigma < 0.26$ eV is displayed in turquoise. For NS and IS, the astrophysical limit values of 0.12 eV, 0.26 eV [37], and 0.9 eV [38] are indicated by red and blue dots, respectively.

and the effective number of neutrino species $N_{\rm eff}$. With the progress in precision cosmology, corresponding bounds on neutrino masses have been dramatically improved. The Planck collaboration has established robust bounds from cosmic-microwave-background power spectra alone: $\Sigma < 0.26$ eV (95% CL), which can be further improved to $\Sigma < 0.12$ eV (95% CL) by including lensing and baryon-acoustic-oscillation data [37]. The Planck satellite data also reveals $N_{\rm eff} = 2.99 \pm 0.17$, in agreement with the SM prediction. It is worth noting that, in the case of decaying neutrinos, a value of Σ as large as 0.9 eV is still allowed by the data [38]. In Fig. 3, Σ is presented as a function of mass of the lowest eigenstate m_0. From the figure, it is seen that cosmological measurements are close enough to rule out the inverted spectrum of neutrino masses.

2.2.1 Effect of nuclear medium on $m_{\beta\beta}$. Recently, the possible effect of the nuclear medium on 0νββ-decay was considered

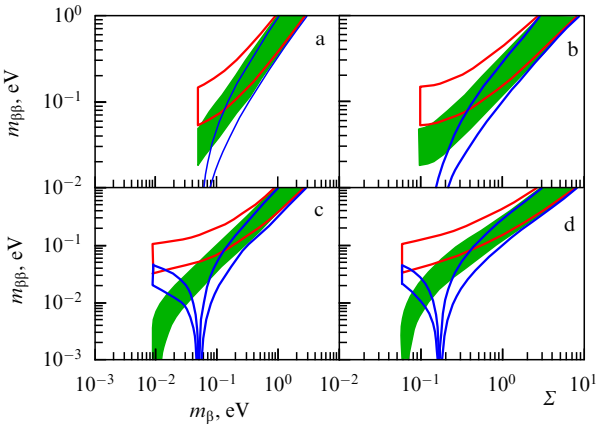

Figure 4. (Color online.) Allowed range of values for effective Majorana mass $m_{\beta\beta}$ as a function of the effective electron neutrino mass m_β (a, c) and sum of neutrino masses Σ (b, d). Figures a, b and c, d correspond to cases of inverted and normal spectra of neutrino masses, respectively. Green, red, and blue bands refer to values $\langle \bar{q}q\rangle g = 0$ (vacuum), 0.1, and -0.05 eV, respectively.

[40]. It was proposed that the neutrino mixing and masses in the nucleus can differ significantly from those in a vacuum if there are exotic particles, preferably scalars, which interact with the neutrinos. The nuclear matter effect on the $0\nu\beta\beta$-decay rate can be calculated in the mean field approach [40].

The effective lepton number violating the four-fermion neutrino-quark Lagrangian with the operators of the lowest dimension can be written as

$$\mathcal{L}_{\rm eff} = \frac{1}{\Lambda^2_{\rm LNV}} \sum_{i,j,{\rm q}} \left(g^{\rm q}_{ij} \overline{\nu^C_{{\rm L}i}} \nu_{{\rm L}j} \bar{\rm q}{\rm q} + {\rm H.c.} \right), \tag{12}$$

where the fields $\nu_{{\rm L}i}$ are the active neutrino left-handed flavor states, and $g^{\rm q}_{ij}$ are their dimensionless couplings to the scalar quark currents with $i, j = {\rm e}, \mu, \tau$.

For the sake of simplicity, we consider the case of a scalar coupling such that $2\hat{g}_{ij}/\Lambda^2_{\rm LNV} = \delta_{ij} g$, where $\hat{g} = U^\dagger g^{\rm q} U$. In this case, the effective Majorana mass is

$$m_{\beta\beta} = \left| \sum_{i=1}^{3} (U_{{\rm e}i})^2 \xi_i |m_i - \langle \bar{q}q\rangle g| \right|. \tag{13}$$

The Majorana phase factor ξ_i is given in [40].

With the above simplification, the quantity $m_{\beta\beta}$ in a nuclear medium, in contrast to the one in a vacuum, depends on the new unknown parameter g. The unknown phases in Eqn (13) are varied in the interval $[0, 2\pi]$. In Fig. 4, $m_{\beta\beta}$ is expressed as a function of directly observable parameters, namely m_β and Σ. The best-fit values of vacuum mixing angles and the neutrino mass squared differences are taken from [36]. In the upper and lower panels, green, red, and blue bands refer to values $\langle \bar{q}q\rangle g = 0$ (vacuum), 0.1, and -0.05 eV, respectively. We see that in-medium ($g \neq 0$) values of $m_{\beta\beta}$ differ significantly from those for a vacuum ($g = 0$). If in the future gradually improving limits on m_β and Σ come into conflict with possible evidence of the $0\nu\beta\beta$-decay represented by $m_{\beta\beta}$ in a vacuum, new physics would be mandatory. A possible explanation could be the generation of in-medium Majorana neutrino mass due to nonstandard interactions of neutrinos with nuclear matter of decaying nuclei.

2.3 Neutrino mixing scenarios with sterile neutrinos

Several theories beyond the SM predict the existence of new types of neutrinos, so-called sterile neutrinos, which owe their name to the fact that they do not take part in any SM interaction. Right-handed partners for known purely left-handed neutrinos are an example of such sterile neutrinos. While the number of active neutrinos is known to be three $(\nu_{\rm e}, \nu_\mu, \nu_\tau)$, it is not known how many mass states are contained in these flavor states.

The most general $(3+n)\times(3+n)$ Dirac–Majorana neutrino mass matrix in the basis of 3 active left-handed $(\nu'_{\rm eL}, \nu'_{\mu{\rm L}}, \nu'_{\tau{\rm L}})$ and n sterile right-handed $(N'^C_{1{\rm R}}, \ldots, N'^C_{n{\rm R}})$ neutrino states takes the form

$$\begin{aligned}\mathcal{L}_{\rm D+M} &= -\frac{1}{2} \begin{pmatrix} \overline{\nu'^C_{\rm L}} & \overline{N'_{\rm R}} \end{pmatrix} \begin{pmatrix} M_{\rm L} & M_{\rm D} \\ M^{\rm T}_{\rm D} & M_{\rm R} \end{pmatrix} \begin{pmatrix} \nu'_{\rm L} \\ N'^C_{\rm R} \end{pmatrix} + {\rm H.c.} \\ &= -\frac{1}{2} \sum_{i=1}^{3} m_i \overline{\nu_i} \nu_i + \sum_{k=1}^{n} M_k \overline{N_k} N_k \,. \end{aligned} \tag{14}$$

Here, $M_{\rm L,R}$ and $M_{\rm D}$ are Majorana and Dirac mass terms, respectively. The mass matrix is diagonalized by the unitary matrix

$$\mathcal{U} = \begin{pmatrix} U & S \\ T & V \end{pmatrix}, \tag{15}$$

which is a generalization of the PMNS matrix. After diagonalization, one ends up with 3 light ν_i $(i = 1, 2, 3)$ and n heavy N_k $(k = 1, \ldots, n)$ Majorana neutrino mass eigenstates with masses m_i and M_k, respectively.

2.3.1 3+1 active-sterile neutrino mixing scenario. This $3+1$ mixing scenario implies that there are 3 light neutrinos (with masses m_1, m_2, and m_3) and a single heavy neutrino with unknown mass $M_1 = m_{\rm h}$ in a range from the eV to GUT scale. In the presence of a single sterile neutrino, the $U(4\times 4)$ neutrino mixing matrix becomes

$$U = \begin{pmatrix} U_{\rm e1} & U_{\rm e2} & U_{\rm e3} & U_{\rm e4} \\ U_{\mu 1} & U_{\mu 2} & U_{\mu 3} & U_{\mu 4} \\ U_{\tau 1} & U_{\tau 2} & U_{\tau 3} & U_{\tau 4} \\ U_{\rm s1} & U_{\rm s2} & U_{\rm s3} & U_{\rm s4} \end{pmatrix} = R_{34} \tilde{R}_{24} \tilde{R}_{14} R_{23} \tilde{R}_{13} R_{12} P \,. \tag{16}$$

It depends on 6 mixing angles (θ_{14}, θ_{24}, θ_{34}, θ_{12}, θ_{13}, θ_{23}) and 3 Dirac (δ_{24}, δ_{14}, δ_{13}) and 3 Majorana (α_1, α_2, α_3) CP-violating phases entering the diagonal P matrix, $P = {\rm diag}\,(\exp(i\alpha_1), \exp(i\alpha_2), \exp[i(\alpha_3 + \delta_{13})], \exp(i\delta_{14}))$.

The phenomenology of the fourth neutrino depends on its hypothetical mass value. The main target of ongoing experimental efforts is sterile neutrinos with a mass of the order of eV [41], which can solve a number of anomalies found in neutrino oscillation experiments. The LSND [42], MiniBooNE [43], and Neutrino-4 [44] collaborations have made observations consistent with a nonstandard neutrino that does not interact weakly. Moreover, both the GALLEX [45] and SAGE [46] experiments reported a deficit of neutrinos from ^{37}Ar and ^{51}Cr electron-capture decays — the gallium anomaly. A re-examination of antineutrinos emitted from nuclear reactors revealed a significant discrepancy between measured and expected fluxes at $\leqslant 100$ m — the reactor antineutrino anomaly [47].

A keV-scale heavy neutrino is a viable candidate for warm dark matter, as it may be long-lived to survive till the present with a lifetime exceeding the age of the Universe. The

strongest experimental bounds on the existence of keV-scale sterile neutrino dark matter are currently obtained from astrophysical observations with telescopes that search for a mono-energetic X-ray line arising from the decay of relic sterile neutrinos. These measurements limit the active-to-sterile mixing amplitude indicated as $|U_{e4}|^2 < 10^{-6}-10^{-10}$ in a mass range of 1–50 keV [48, 49].

Very heavy, typically $\mathcal{O}(10^{14}$ GeV), sterile neutrinos provide a natural explanation for the light mass of active neutrinos via the seesaw mechanism and could shed light on the matter–antimatter asymmetry of the Universe via leptogenesis.

2.3.2 Seesaw scenario with 3 sterile neutrinos. In left-right symmetric models, $n = 3$. The smallness of m_i can be guaranteed by the seesaw-I condition $M_R \gg M_D$. As is well known, this leads to very heavy states N_k with masses $M_k \gg 1$ TeV being beyond the experimental reach. The 6×6 unitary neutrino mixing matrix [50] is formed with 3×3 block matrices in flavor space U, S, T, V and is completely parameterized with 15 angles and 10 Dirac (δ_{46}, δ_{36}, δ_{35}, δ_{26}, δ_{25}, δ_{24}, δ_{16}, δ_{15}, δ_{14}, and δ_{13}) and 5 Majorana (α_1, α_2, α_3, α_4, and α_5) CP violating phases:

$$U = R_{56}\tilde{R}_{46}R_{45}\tilde{R}_{36}\tilde{R}_{35}R_{34} \times \tilde{R}_{26}\tilde{R}_{25}\tilde{R}_{24}R_{23}\tilde{R}_{16}\tilde{R}_{15}\tilde{R}_{14}\tilde{R}_{13}R_{12}P\,, \quad (17)$$

where

$$P = \mathrm{diag}\left(\exp(\mathrm{i}\alpha_1), \exp(\mathrm{i}\alpha_2), \exp[\mathrm{i}(\alpha_3+\delta_{13})], \exp[\mathrm{i}(\alpha_4+\delta_{14})], \exp[\mathrm{i}(\alpha_5+\delta_{15})], \exp(\mathrm{i}\delta_{16})\right).$$

Of course, it is practically impossible to get phenomenological information about the involved mixing angles and phases without any assumptions.

If for the sake of simplicity the universality of flavor mixing between active and sterile neutrino sectors is assumed and the unitarity of the seesaw mixing matrix $\mathcal{U}$ is exploited, it can be written as [51]

$$\mathcal{U} = \frac{1}{\sqrt{1+\zeta^2}}\begin{pmatrix} U & \zeta\,\mathbb{1} \\ -\zeta\,\mathbb{1} & U^\dagger \end{pmatrix}. \quad (18)$$

Here, $\zeta = m_D/m_{LNV}$, where m_D is the typical scale of charged leptons masses and m_{LNV} is the LNV scale of the order of the Majorana masses M_i of heavy neutrinos. A small violation of the unitarity of the U matrix is beyond the current accuracy of phenomenological determination of elements of the PMNS matrix. Thus, U is identified with the PMNS matrix. Surprisingly, mixing in the heavy neutrino sector is governed by the $U^\dagger$ mixing matrix [51], which takes the form

$$U^\dagger = \begin{pmatrix} c_{12}\,c_{13}\,\exp(-\mathrm{i}\alpha_1) & \left[-s_{12}\,c_{23} - c_{12}\,s_{13}\,s_{23}\,\exp(-\mathrm{i}\delta)\right]\exp(-\mathrm{i}\alpha_1) & \left[s_{12}\,s_{23} - c_{12}\,s_{13}\,c_{23}\,\exp(-\mathrm{i}\delta)\right]\exp(-\mathrm{i}\alpha_1) \\ s_{12}\,c_{13}\,\exp(-\mathrm{i}\alpha_2) & \left[c_{12}\,c_{23} - s_{12}\,s_{13}\,s_{23}\,\exp(-\mathrm{i}\delta)\right]\exp(-\mathrm{i}\alpha_2) & \left[-c_{12}\,s_{23} - s_{12}\,s_{13}\,c_{23}\,\exp(-\mathrm{i}\delta)\right]\exp(-\mathrm{i}\alpha_2) \\ s_{13}\,\exp(\mathrm{i}\delta) & c_{13}\,s_{23} & c_{13}\,c_{23} \end{pmatrix}. \quad (19)$$

The elements of the 6×6 Dirac–Majorana mass matrix $\mathcal{M}$ can be calculated as follows:

$$\mathcal{M} = \begin{pmatrix} M_L & M_D \\ M_D^T & M_R \end{pmatrix} = \begin{pmatrix} U & \zeta\,\mathbb{1} \\ -\zeta\,\mathbb{1} & U^\dagger \end{pmatrix}^* \begin{pmatrix} m & 0 \\ 0 & M \end{pmatrix}^* \begin{pmatrix} U & \zeta\,\mathbb{1} \\ -\zeta\,\mathbb{1} & U^\dagger \end{pmatrix}^\dagger. \quad (20)$$

Here, m and M stand for diagonal 3×3 mass matrices $m = \mathrm{diag}(m_1, m_2, m_3)$ and $M = \mathrm{diag}(M_1, M_2, M_3)$, respectively; $1/(1-\zeta^2)^{1/2} \simeq 1$ is assumed. The explicit form of the elements of $\mathcal{M}$ is given in [51].

2.3.3 Quasi-Dirac neutrinos with 3 sterile neutrinos. If the Dirac–Majorana mass term is dominated by Dirac masses, one ends up with six Majorana neutrino states with pairwise quasi-degenerate masses, referred to as quasi-Dirac neutrinos [52–56]. It is a scenario opposite to the above see-saw case with 3 light and 3 heavy neutrinos.

The six quasi-Dirac neutrino mass eigenvalues $m_i^\pm$ can be written as

$$m_i^\pm = \pm m_i + \epsilon_i\,. \quad (21)$$

The Dirac masses m_i $(i = 1, 2, 3)$ correspond to those obtained by a diagonalization of the Dirac mass matrix M_D by a bi-unitary transformation ($U^\dagger U = \mathbb{1} = V^\dagger V$ is assumed),

$$U^\dagger M_D V \equiv \begin{pmatrix} m_1 & 0 & 0 \\ 0 & m_2 & 0 \\ 0 & 0 & m_3 \end{pmatrix}, \quad (22)$$

and 3 mass splittings ϵ_i are Majorana components of the masses of quasi-Dirac neutrinos.

The unitary matrix $\mathcal{U}$, which diagonalizes the Dirac–Majorana mass matrix, can be written as [57]

$$\mathcal{U} = \frac{1}{\sqrt{2}}\begin{pmatrix} (\mathbb{1}+X^\dagger)U^T & -(\mathbb{1}-X^\dagger)V^\dagger \\ (\mathbb{1}-X)U^T & (\mathbb{1}+X)V^\dagger \end{pmatrix} + \mathcal{O}(X^2), \quad (23)$$

where X is a 3×3 general matrix. Each of unitary matrices U and V contain is determined by three angles and three phases. The remaining nine angles and nine phases are included in the matrix X, for which the perturbative expansion is considered. The pure Dirac case is reproduced for $X = 0$.

The effect of small mass splitting can be studied by considering universal Majorana mass splitting ϵ ($\epsilon_i = \epsilon$) and $X = 0$, which allows agreement with the current phenomenology of neutrino oscillations. Due to this assumption, the neutrino mass spectrum can be completely fixed by fitting all oscillation frequencies given by five independent mass-squared differences. It should be kept in mind that, in the general case with three independent mass splittings ϵ_i, the neutrino mass spectrum depends on six parameters (m_i and ϵ_i with $i = 1, 2, 3$) and cannot be determined using the formalism of neutrino oscillations, which only depends on five differences of masses squared, i.e., one degree of freedom is missing.

The probability of oscillations of 3 flavor neutrinos (ν_e, ν_μ, ν_τ) can be described with eight parameters, namely three angles (θ_{12}, θ_{13}, and θ_{23}) and one Dirac CP phase δ having its origin in a single unitary matrix, two mass squared differences (Δm^2_{21} and Δm^2_{31}), the lightest neutrino mass (m_1

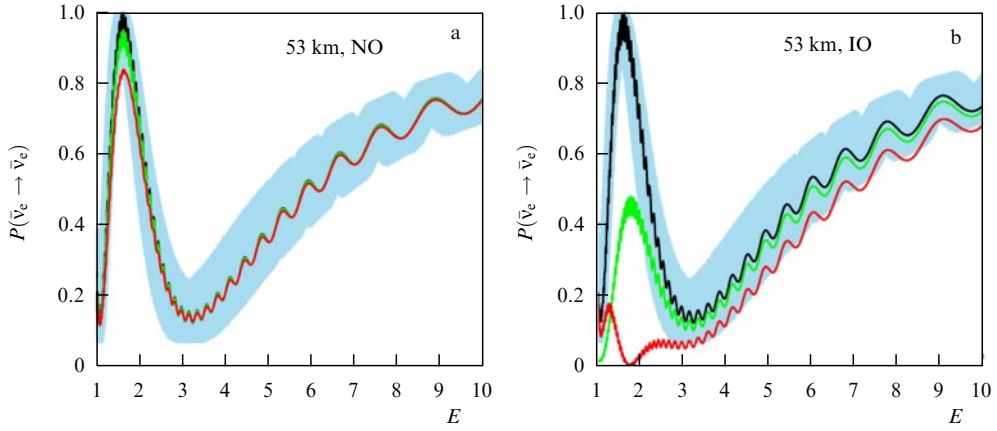

Figure 5. (Color online.) Survival probabilities of $\bar{\nu}_e$ as functions of energy E for 53-km baselines. Plots in panels a and b correspond to normal (NO) and inverted (IO) mass orderings, respectively. Probabilities are shown for three cases: $\epsilon = 0$, 3ν mixing case, $\epsilon = 10^{-4}$ eV, and $\epsilon = 2 \times 10^{-4}$ eV, by black, green, and red lines, respectively. Lightest Dirac mass is 0.01 eV. Cyan bands represent $\bar{\nu}_e$ survival probabilities in three-flavor neutrino oscillation framework, with 3σ the allowed range of oscillation parameters. Benchmark values of oscillation parameters and their allowed ranges of 3σ, as used in this study, are given in Table 1.

for normal ordering and m_3 for inverted ordering of Dirac neutrino masses), and a small Majorana neutrino mass parameter ϵ. It should be recalled that, within the commonly considered mixing scheme of three neutrinos, the required number of parameters is only two fewer (three mixing angles, one phase, and two mass squared differences).

The expression of $\bar{\nu}_e$ survival probability is given by [57],

$$P_{\bar{\nu}_e \to \bar{\nu}_e}(\epsilon \neq 0) = 1 - P_1 - 4\, c_{13}^4 c_{12}^2 s_{12}^2 F_{21} - 4\, s_{13}^2 c_{13}^2 (c_{12}^2 F_{31} + s_{12}^2 F_{32}) \quad (24)$$

with

$$P_1 = c_{13}^4 c_{12}^4 \sin^2 \frac{m_1 \epsilon L}{E} + c_{13}^4 s_{12}^4 \sin^2 \frac{m_2 \epsilon L}{E} + s_{13}^4 \sin^2 \frac{m_3 \epsilon L}{E}\,, \quad (25)$$

$$F_{ij} = \frac{1}{4}\left(\sin^2 \frac{\Delta m_{ij}^2 + 2\epsilon \Delta m_{ij}}{4E} L + \sin^2 \frac{\Delta m_{ij}^2 - 2\epsilon \Delta m_{ij}}{4E} L + \sin^2 \frac{\Delta m_{ij}^2 + 2\epsilon \sum m_{ij}}{4E} L + \sin^2 \frac{\Delta m_{ij}^2 - 2\epsilon \sum m_{ij}}{4E} L \right). \quad (26)$$

Here, $\Delta m_{ij} = m_i - m_j$, $\sum m_{ij} = m_i + m_j$, $\Delta m_{ij}^2 = m_i^2 + m_j^2$, and L is the baseline.

An analysis of the lightest Dirac neutrino mass and ϵ of the $3+3$ quasi-Dirac neutrino mixing scheme was performed by exploiting the 1σ and 3σ uncertainty of measured probability of $\bar{\nu}_e$ oscillations from a reactor. The mixing angles θ_{12}, θ_{13} and mass squared differences Δm_{21}^2 and Δm_{31}^2 were considered to be those determined within the PMNS unitary mixing scheme with three neutrinos. It was found that a tiny value of ϵ below 1 meV does not affect the current phenomenology representing, e.g., the Daya Bay experiment, but can have a significant impact on the JUNO experiment registering oscillations of antineutrinos at significantly larger distances [57].

In Fig. 5, the survival probability of an electron antineutrino as a function of energy is shown for a 53-km baseline relevant for the medium-baseline JUNO reactor neutrino oscillation experiment. Results are shown for three cases: (i) $\epsilon = 0$, 3ν mixing case, (ii) $\epsilon = 10^{-4}$ eV, and (iii) $\epsilon = 2 \times 10^{-4}$ by black, green, and red lines, respectively. The plot shown in Fig. 5a(b) corresponds to normal (inverted) ordering for which m_1 (m_3) is the lightest Dirac mass. A detailed study on restricting ϵ, which depends on the considered value of the lightest neutrino mass and ordering of neutrinos (normal or inverted) was presented in [57].

Within the considered simplification, the effective Majorana mass measured in $0\nu\beta\beta$-decay experiments,

$$m_{\beta\beta} = \left| \sum_{i=1}^{3} U_{ei}^2 \epsilon \right| = |\epsilon| \left| c_{12}^2 c_{13}^2 + \exp(2i\alpha_{21}) c_{13}^2 s_{12}^2 + \exp(2i\alpha_{31}) s_{13}^2 \right|, \quad (27)$$

is directly proportional to the Majorana component of neutrino masses ϵ. For normal (inverted) ordering of neutrino masses, the upper limit $m_{\beta\beta} < 30$ meV ($m_{\beta\beta} < 10$ meV) was obtained by exploiting the current neutrino oscillation phenomenology [57].

The effective electron neutrino mass for single beta decay takes the form

$$m_\beta = \left(\sum_{i=1}^{3} |U_{ei}|^2 (m_i^2 + \epsilon^2) \right)^{1/2} = \sqrt{m_1^2 c_{12}^2 c_{13}^2 + m_2^2 c_{13}^2 s_{12}^2 + m_3^2 s_{13}^2 + \epsilon^2}\,. \quad (28)$$

We see that, for ϵ in the range of a few meV, m_β is slightly larger in the case of six quasi-Dirac neutrinos when compared with the conventional case of three Dirac neutrinos.

Within the considered simplified scenario, the quantity Σ measured in cosmological observations is insensitive to universal mass splitting ϵ. We have

$$\Sigma = \frac{1}{2} \sum_{i=1}^{6} |\widetilde{\mathcal{M}}_{ii}| = \sum_{i=1}^{3} m_i\,. \quad (29)$$

The factor of $1/2$ reflects the quasi-Dirac (or Dirac) nature of neutrinos. Only three out of their six states are kept in equilibrium with the cosmological plasma of the early Universe by $V-A$ interactions of the SM.

3. Measurement of neutrino mass with single β-decay and electron capture

The measurement of the electron spectrum in β-decays provides a reliable direct determination of the values of neutrino masses. The history of the neutrino mass search started with Enrico Fermi's article [58] a long time ago in 1934. He pointed out that the neutrino mass value manifests itself in the shape of the β-decay spectrum, namely, close to the kinematical end point. Already in 1938, A I Alichanian, A I Alichanow, and B S Dželepow carried out the first experimental search for the neutrino mass by measuring the β-spectrum shape of ^{210}Bi [59].

3.1 β-decay of tritium

The most sensitive experiments use the super-allowed β-decay of tritium,

$$^3\mathrm{H} \to {}^3\mathrm{He} + \mathrm{e}^- + \overline{\nu}_\mathrm{e}\,, \tag{30}$$

to search for the effect of neutrino masses m_k $(k = 1, 2, 3)$ near the endpoint of the electron spectrum, where $Q - T_\mathrm{e} \sim m_k$; $Q = 18.6$ keV and T_e are the Q-value of the process and electron kinetic energy, respectively. A low Q-value is important, because the relative number of events occurring in the energy range ΔT_e near the endpoint is proportional to $(\Delta T_\mathrm{e}/Q)^3$. Due to the short half-life of 12.3 years, high decay rates can be achieved with reasonable amounts of tritium.

The commonly presented form of the electron energy spectrum for tritium β-decay is

$$N(E_\mathrm{e}) = \frac{\mathrm{d}\Gamma}{\mathrm{d}E_\mathrm{e}} = \frac{G_\mathrm{F}^2 V_\mathrm{ud}^2}{2\pi^3}\, B_{^3\mathrm{H}} F(Z, E_\mathrm{e}) p_\mathrm{e} E_\mathrm{e} (E_0 - E_\mathrm{e}) \times \sum_k |U_{\mathrm{e}k}|^2 \sqrt{(E_0 - E_\mathrm{e})^2 - m_k^2}\, \theta(E_0 - E_\mathrm{e} - m_k)\,, \tag{31}$$

where $B_{^3\mathrm{H}}$ is the sum of squared Fermi and Gamow–Teller matrix elements weighted with squared vector g_V and axial vector g_A coupling constants, respectively:

$$B_{^3\mathrm{H}} = g_\mathrm{V}^2 |M_\mathrm{F}|^2 + g_\mathrm{A}^2 |M_\mathrm{GT}|^2\,. \tag{32}$$

Here, G_F is the Fermi constant and V_ud is an element of the Cabbibo–Kobayashi–Maskawa (CKM) matrix, and p_e, E_e, and E_0 are the momentum, energy, and maximal endpoint energy (in the case of zero neutrino mass) of the electron, respectively. $F(Z, E)$ denotes the relativistic Coulomb factor.

The drawback of the conventional expression for the differential decay rate in Eqn (31) is that nuclear recoil is not taken into account. The relativistic expression for the maximal electron energy

$$E_\mathrm{e}^\mathrm{max} = \frac{1}{2M_f}\left[M_i^2 + m_\mathrm{e}^2 - (M_f + m_k)^2\right] \tag{33}$$

gives a value about 3.4 eV lower than the considered approximation $E_\mathrm{e}^\mathrm{max} \simeq E_0 = M_i - M_f - m_k$ (M_i, M_f, and m_e are masses of the tritium atom, $^3\mathrm{He}^+$, and the electron, respectively).

The effect of nuclear recoil was taken into account in a relativistic treatment of the β-decay spectrum of tritium [60] derived in the elementary particle treatment of weak interaction [61–63]. Advantage was taken of the fact that the spin-isospin characteristics of the ^{3}H (^{3}He) nucleus and neutron (proton) are the same. The differential decay rate was found to be of the form [60]

$$\begin{aligned}\frac{\mathrm{d}\Gamma}{\mathrm{d}E_\mathrm{e}} = {}& \frac{1}{2\pi^3}(G_\mathrm{F} V_\mathrm{ud})^2 F(Z, E_\mathrm{e})\, p_\mathrm{e} \\ & \times \frac{M_i^2}{m_{12}^2} \sum_k |U_{\mathrm{e}k}|^2 \sqrt{y\left(y + 2m_k \frac{M_f}{M_i}\right)} \\ & \times \left[(g_\mathrm{V} + g_\mathrm{A})^2 y \left(y + m_k \frac{M_f}{M_i}\right) \frac{M_i^2 (E_\mathrm{e}^2 - m_\mathrm{e}^2)}{3m_{12}^4}\right. \\ & \times (g_\mathrm{V} + g_\mathrm{A})^2 \left(y + m_k \frac{M_f + m_k}{M_i}\right) \frac{M_i E_\mathrm{e} - m_\mathrm{e}^2}{m_{12}^2} \\ & \times \left(y + M_f \frac{M_f + m_k}{M_i}\right) \frac{M_i^2 - M_i E_\mathrm{e}}{m_{12}^2} \\ & - (g_\mathrm{V}^2 - g_\mathrm{A}^2) M_f \left(y + m_k \frac{M_f + m_k}{M_i}\right) \frac{M_i E_\mathrm{e} - m_\mathrm{e}^2}{m_{12}^2} \\ & \left. + (g_\mathrm{V} - g_\mathrm{A})^2 E_\mathrm{e} \left(y + m_k \frac{M_f}{M_i}\right)\right] \theta(E_\mathrm{e}^\mathrm{max} - E_\mathrm{e} - m_k)\,, \end{aligned} \tag{34}$$

where $m_{12}^2 = M_i^2 + m_\mathrm{e}^2 - 2M_i E_\mathrm{e}$, $y = E_\mathrm{e}^\mathrm{max} - E_\mathrm{e}$, $g_\mathrm{V} = 1$, and $g_\mathrm{A} = 1.247$ [60]. By keeping only the dominant contributions and by introducing a mass scale parameter M instead of M_i and M_f, we end up with

$$\begin{aligned}\frac{\mathrm{d}\Gamma}{\mathrm{d}E_\mathrm{e}} \simeq {}& \frac{1}{2\pi^3}(G_\mathrm{F} V_\mathrm{ud})^2 F(Z, E_\mathrm{e})\, p_\mathrm{e} E_\mathrm{e} (g_\mathrm{V}^2 + 3g_\mathrm{A}^2) \\ & \times \sum_k |U_{\mathrm{e}k}|^2 \sqrt{y(y + 2m_k)}\,(y + m_k)\,. \end{aligned} \tag{35}$$

For the relativistic form of the Kurie function, we get

$$K(y, m_k) = \frac{G_\mathrm{F} V_\mathrm{ud}}{\sqrt{2\pi^3}} \sqrt{g_\mathrm{V}^2 + 3g_\mathrm{A}^2} \left(\sqrt{y(y + 2m_k)}\,(y + m_k)\right)^{1/2}. \tag{36}$$

The Kurie plot is linear near the endpoint for zero neutrino mass ($m_k = 0$). However, the linearity of the Kurie plot is lost if the neutrino has a nonzero mass. Deviation from a straight line depends on neutrino mass m_k.

3.1.1 Model with 3 light neutrinos ($\mathbf{m_k < 1}$ eV, $\boldsymbol{k = 1, 2, 3}$). If the masses of 3 light neutrinos are in the sub-eV region and $m_k \ll E^\mathrm{max} - E_\mathrm{e}$, the Kurie function can be written as

$$\begin{aligned} K(y) = {}& \sum_k |U_{\mathrm{e}k}|^2 K(y, m_k) \simeq \frac{G_\mathrm{F} V_\mathrm{ud}}{\sqrt{2\pi^3}} \sqrt{g_\mathrm{V}^2 + 3g_\mathrm{A}^2} \\ & \times \left((y + m_\beta)\sqrt{y(y + 2m_\beta)}\right)^{1/2}, \end{aligned} \tag{37}$$

where $y = (E_0 - E_\mathrm{e} - m_\beta)$.

Usually, the primary molecule is T_2, which, after the decay of a tritium nucleus, becomes a molecule of $\mathrm{T}\,^3\mathrm{He}$. With a probability of about 43%, $\mathrm{T}\,^3\mathrm{He}$ does not go into its ground state. Then, electron energy distribution is given by the sum of partial energy distributions associated with all molecule final states i:

$$\frac{\mathrm{d}\Gamma}{\mathrm{d}E_\mathrm{e}}(E_\mathrm{e}, E_0, m_\beta) = \sum_i P_i \frac{\mathrm{d}\Gamma}{\mathrm{d}E_\mathrm{e}}(E_\mathrm{e}, E_0 - \varepsilon_i, m_\beta)\,. \tag{38}$$

Here, ε_i is the energy of the excited state (for ground state $\epsilon_0 = 0$) and P_i is its probability ($\sum_i P_i = 1$).

The study of the β-decay of molecular tritium has become the source of the most accurate data on the magnitude of the neutrino mass. In 1940, Geoff Hanna and Bruno Pontecorvo used a proportional chamber filled with tritium to evaluate the rest mass of the neutrino experimentally at the Chalk River Institute (Canada) [64]. A limit of ~ 1 keV on the neutrino mass was obtained, which corresponds to the resolution of the detector. In the work by Bergkvist et al. [65], the limit was set down to $m_\beta < 55-60$ eV. The excitation of the residual ion was taken into account as a source of the main systematic corrections.

The increase in measurement sensitivity achieved over the past 30 years is associated with the invention of an electrostatic spectrometer with adiabatic magnetic collimation [66, 67]. The principle of operation of the spectrometer is based on the adiabaticity of the movement of an electric charge in a slowly varying magnetic field. When moving from a strong magnetic field to a weak one, the charges move along the magnetic field lines, lining up along their direction. It is important that the spectrometer resolution does not depend on the transverse dimensions of the tritium source.

The Troitsk (Russia) [68, 69] and Mainz (Germany) [70] experiments used molecular tritium and the magnetic adiabatic collimation technique to set the previous most stringent direct upper limit at $m_\beta < 2.2$ and 2.3 eV (95% CL), respectively, with a high-accuracy shape measurement of the β-decay spectrum in the vicinity of its kinematic endpoint. As a result of this success, the KATRIN experiment was designed [39] and constructed with the primary goal of either setting an improved upper limit on m_β with an unprecedented sub-eV sensitivity or discovering its value through a measurement of the tritium beta-decay spectrum close its to its endpoint, where the imprint of the neutrino mass is maximal.

KATRIN is the most precise neutrino mass experiment currently in operation. The detector is a combination of a gaseous molecular tritium source with a high activity of 10^{11} decays per second and a spectrometer of high resolution with $\Delta E = 1$ eV. The β-electrons are guided along magnetic field lines from a windowless gaseous tritium source to the spectrometer, which is operated as a magnetic adiabatic collimation and electrostatic filter [66, 67]. The rate of electrons is determined using a pixel focal plane detector situated at the exit of the KATRIN spectrometer. Recent measurements from the KATRIN experiment present an effective neutrino mass square value,

$$m_\beta^2 = \left(-1.0^{+0.9}_{-1.1}\right) \text{eV}^2 , \tag{39}$$

from which an upper bound on the electron neutrino mass m_β of 1.1 eV (90% CL) was established [71]. The completion of the neutrino mass measurement is expected in 2025.

Two other experiments, Project 8 [72] and PTOLEMY [73], which are presently in the R&D phase, are expected to precisely measure the endpoint region of the electron spectrum in the ^{3}H β-decay with a sub-eV sensitivity to the neutrino mass. The Project 8 collaboration aims to measure the absolute neutrino mass scale using cyclotron radiation emission spectroscopy on the beta decay of tritium. The second phase of the project is currently taking data on molecular tritium beta decays, and an analysis is in progress. The main goal is to establish the absolute neutrino mass with a sensitivity down to 40 meV when using atomic tritium as a source [74].

3.1.2 3 + 1 model with light sterile neutrino in eV range. Another purpose of the experiment is to find evidence of possible sterile neutrino states, given the resulting distortion they might cause to the tritium electron spectrum.

In the Troitsk nu-Mass tritium experiment, based on data re-analysis of direct electron antineutrino mass measurements, which included an extra 100 eV spectrum interval at lower energies, a search for any sign of an additional light sterile neutrino in a mass range of up to 100 eV was performed. The upper limit for the contribution of a heavy eigenstate to the electron neutrino was found to be around or less than 1% (at 95% CL) for neutrino masses above 20 eV [75]. On the contrary, from the Mainz experiment data, it was concluded that mixing the fourth neutrino with the electron neutrino is compatible with zero and only a small fraction of the parameter space for such a fourth neutrino mass state favored by the attempt to explain reactor neutrino and related anomalies was constrained [76].

Recently, the KATRIN collaboration reported on the light sterile neutrino search from the first four-week science run of the KATRIN experiment in 2019. In a framework with three active neutrinos and one sterile neutrino, β-decay electrons with energy down to 40 eV below the endpoint in the absence of neutrino mass effects were analyzed. No significant sterile neutrino signal was observed. For the mass of the fourth neutrino state, limits in the range $m_4^2 \leqslant 1000\,\text{eV}^2$ and exclusion bounds on the active-to-sterile neutrino mixing parameter $|U_{e4}|^2$ were presented. The best sensitivity was found at $m_4 \sim 20$ eV, allowing the limit [77]

$$|U_{e4}|^2 \geqslant 2 \times 10^{-2} . \tag{40}$$

The obtained new limits supersede the Mainz results for $m_4^2 \leqslant 1000$ eV^2 and improve the Troitsk bound for $m_4^2 < 30\,\text{eV}^2$.

3.1.3 3 + 1 model with light sterile neutrino in keV range. A fourth neutrino mass state with a mass of few keV is a warm dark matter candidate. With an endpoint of $E_0 = 18.6$ keV, the β-decay of tritium is also well suited for a direct search for neutrinos with a mass in the keV range. However, reasonable amounts of tritium are required. A widely used method is based on high-precision measurements of the β-decay spectrum, which is a superposition of spectra corresponding to the different neutrino mass states that comprise the electron neutrino flavor eigenstate. Due to the tiny mass differences among the three light neutrino mass eigenstates, this superposition cannot be resolved with current experimental techniques. A kink-like keV-neutrino signature would be a distinct feature in the otherwise fully smooth tritium β-decay spectrum. The position of the kink depends on the mass of the heavy neutrino m_h, and the signal strength of the broad distortion is governed by the active-sterile mixing amplitude $\sin^2\theta$. The total differential tritium β-decay spectrum can be written as

$$\frac{d\Gamma}{dE} = U_{e4}^2 \frac{d\Gamma}{dE}(m_\beta^2) + (1 - U_{e4}^2) \frac{d\Gamma}{dE}(m_h^2) . \tag{41}$$

The Troitsk nu-Mass experiment established upper limits on the active-sterile mixing amplitude U_{e4}^2 in the mass range of 0.1 to 2 keV, e.g., for $m_h = 1$ keV the bound $U_{e4}^2 < 3 \times 10^{-3}$ was achieved [78]. On the contrary, the Mainz Neutrino Mass Experiment constrained only a small fraction of the parameter space for such a fourth neutrino mass state in the range

$3 \leqslant m_h^2 \leqslant 36{,}400\ \mathrm{eV}^2$ [76]. Current laboratory-based limits are orders of magnitudes weaker than astrophysical bounds [49, 79, 80].

For further progress in the field, it was necessary to eliminate the dominant sources of systematic uncertainties due to the detector system. This goal was achieved with the TRISTAN detector integrated into the KATRIN experiment. The objective of the TRISTAN project is to utilize the unprecedented tritium source luminosity of the KATRIN experiment for a high-precision keV-scale sterile neutrino search by extending the experimental setup with a new multi-pixel silicon drift detector system [81, 82]. TRISTAN is currently an R&D effort for an experiment to take place after the completion of the neutrino mass measurement of KATRIN, prospectively in 2025. The requirements for the TRISTAN detector system are an energy resolution of less than 300 eV (FWHM) at 20 keV, a low energy detection threshold of around 1 keV, and the ability to manage high count rates on the order of 10^8 counts per second. The design goal of TRISTAN is to achieve a sensitivity of $U_{eh}^2 < 10^{-6}$. The TRISTAN group is currently developing a detector system. A 7-pixel TRISTAN prototype detector was already successfully installed for the Troitsk nu-Mass experiment.

3.2 β-decay of rhenium

Compared to tritium, the β-decay of ^{187}Re,

$$^{187}\mathrm{Re} \rightarrow {}^{187}\mathrm{Os} + \mathrm{e}^- + \overline{\nu}_\mathrm{e}\,, \tag{42}$$

has a 7 times lower endpoint energy, 2.47 keV, resulting in a 350 times higher relative fraction of the β-spectrum in the interesting endpoint region. A large isotopic abundance (62.8%) makes it possible to use in the experiment natural rhenium. A disadvantage is the very long half-life of 4.3×10^{10} years and a very complicated electronic structure. It can be compensated for by using a β-emitter in cryobolometers, which measure the entire energy released in the absorber, except that of the neutrino.

The ground-state spin parity is $5/2^+$ for ^{187}Re and $1/2^-$ for the daughter nucleus ^{187}Os, and the decay is associated with $\Delta J^\pi = 2^-$ of the nucleus, i.e., classified as a unique first forbidden β-decay. The theoretical spectral shape of the β-decay of ^{187}Re is given by [83]

$$\begin{aligned}\frac{\mathrm{d}\Gamma}{\mathrm{d}E_\mathrm{e}} &= \frac{\mathrm{d}\Gamma^{\mathrm{p}_{3/2}}}{\mathrm{d}E_\mathrm{e}} + \frac{\mathrm{d}\Gamma^{\mathrm{s}_{1/2}}}{\mathrm{d}E_\mathrm{e}} \\ &= \sum_{k=1}^{3} |U_{\mathrm{e}k}|^2\, \frac{G_\mathrm{F}^2 V_\mathrm{ud}^2}{2\pi^3}\, B_\mathrm{Re} R^2 p_\mathrm{e} E_\mathrm{e} (E_0 - E_\mathrm{e}) \\ &\times \frac{1}{3}\Big[F_1(Z,E_\mathrm{e}) p_\mathrm{e}^2 + F_0(Z,E_\mathrm{e})\big((E_0 - E_\mathrm{e})^2 - m_k^2\big)\Big] \\ &\times \sqrt{(E_0 - E_\mathrm{e})^2 - m_k^2}\, \theta(E_0 - E_\mathrm{e} - m_k)\,. \end{aligned} \tag{43}$$

Here, $F_0(Z,E)$ and $F_1(Z,E)$ are relativistic Fermi functions [85]. The explicit form of the factor B_Re, which involves the squared product of the axial-vector coupling constant and Gamow–Teller type nuclear matrix element, is given in [83]. Its value can be determined from the measured half-life.

The emitted electron and neutrino are expected to be, respectively, in the $\mathrm{p}_{3/2}$ and $\mathrm{s}_{1/2}$ states, or vice versa. The decay rate is the sum of particular decay rates associated with the emission of $\mathrm{s}_{1/2}$ and $\mathrm{p}_{3/2}$ electrons, which depend in a different way on the neutrino mass. From calculations, it follows that $\mathrm{p}_{3/2}$-state electrons are emitted about 10^4 times more than for the emission of $\mathrm{s}_{1/2}$-state electrons [83]. The dominance of emission of $\mathrm{p}_{3/2}$ electrons was also confirmed experimentally [84]. A complete understanding of the distortion of the β-decay spectrum is crucial for experiments aiming at the precise measurement of the neutrino mass.

By assuming $m_k \ll Q - T$, the Kurie function takes the form

$$K(y) \simeq \mathcal{B}_\mathrm{Re}\left((y + m_\beta)\sqrt{y(y + 2m_\beta)}\right)^{1/2}, \tag{44}$$

where

$$\mathcal{B}_\mathrm{Re} = \frac{G_\mathrm{F} V_\mathrm{ud}\sqrt{B_\mathrm{Re}}}{\sqrt{2\pi^3}} \sqrt{\frac{R^2 p_\mathrm{e}^2}{3}\frac{F_1(Z,E_\mathrm{e})}{F_0(Z,E_\mathrm{e})}} \tag{45}$$

with $y = (E_0 - E_\mathrm{e} - m_\beta) \geqslant 0$. The ratio $(p_\mathrm{e}^2 F_1(Z,E_\mathrm{e}))/F_0(Z,E_\mathrm{e})$ depends only weakly on the electron momentum in the case of the β-decay of rhenium. With good accuracy, the factor $\mathcal{B}_\mathrm{Re}$ can be considered to be a constant. For $m_\beta = 0$, the Kurie plot is linear near the endpoint. However, the linearity of the Kurie plot is lost if m_β is not equal to zero.

Calorimetric measurements of the β-decay of rhenium were complementary to those carried out with spectrometers. From the spectrum near the endpoint, the MANU experiment in Genoa and the MiBeta experiment in Milan set an upper limit on the neutrino mass of $m_\beta < 26$ eV [86] and $m_\beta < 15$ eV [87], respectively.

The success of these rhenium experiments has encouraged the micro-calorimeter community to propose the ambitious MARE project based on arrays of rhenium low temperature microcalorimeters with the goal to reach a sensitivity of 0.2 eV to the neutrino mass [88]. However, despite past successful investigation of ^{187}Re, the realization of this project was stopped, as this isotope was found to be not fully compatible with the technical requirements of a high sensitivity neutrino mass measurement experiment, mostly due to the low specific activity and the relative slowness of the thermalization process of materials containing this isotope. For these reasons, the focus of the community has shifted to ^{163}Ho.

3.3 Electron capture of holmium

Neutrino masses can be studied not only with β-decays, in which an electron antineutrino is produced, but also with electron capture processes, where the electron neutrino is in the final state. In order to maximize the number of statistics in the region of interest, decays characterized by low Q-value transition energies are preferable. The best nuclide is ^{163}Ho as it has the smallest energy available of all possible nuclides for electron capture. This energy is given by the difference between the mass of the parent ^{163}Ho and daughter ^{163}Dy atoms and corresponds to $Q_\mathrm{EC} = 2833 \pm 30^{\,\mathrm{stat}} \pm 15^{\,\mathrm{syst}}$ eV [89].

In the electron capture of ^{163}Ho,

$$\mathrm{e}_\mathrm{b}^- + {}^{163}\mathrm{Ho} \rightarrow {}^{163}\mathrm{Dy}^* + \nu_\mathrm{e}\,, \tag{46}$$

a neutrino is emitted, and the daughter atom, ^{163}Dy*, is in an atomic excited state. The isotope ^{163}Ho could be implanted into well-suited cryobolometers. The uppermost end of the electromagnetic de-excitation spectrum of ^{163}Dy looks similar to the endpoint spectrum of β-decay and is sensitive to the neutrino mass.

The calorimetric spectrum is given by

$$\frac{\mathrm{d}\Gamma}{\mathrm{d}E_{\mathrm{c}}} \propto (Q_{\mathrm{EC}} - E_{\mathrm{c}}) \sum_k |U_{ek}|^2 \sqrt{(Q_{\mathrm{EC}} - E_{\mathrm{c}})^2 - m_k^2} \times \sum_f \frac{\gamma_f}{(E_{\mathrm{c}} - E_f)^2 + \gamma_f^2/4} \left| \langle f | \sum_j \Psi_j(R) \hat{e}_j | i \rangle \right|^2 . \quad (47)$$

Here, E_{c} denotes energy deposited in the calorimeter. The dependence on the neutrino mass is due to the neutrino phase-space factor in front of the sum over all final states of the Dysprosium daughter atom. Each contribution to the calorimetric spectrum is determined with width γ_f and position energy E_f. $|i\rangle$ and $|f\rangle$ are the holmium (initial) and dysprosium (final) atomic states, respectively. $\hat{e}_j$ denotes an annihilation operator that removes an electron in orbital $\Psi_j(x)$ from the ground state of holmium. The orbital wave functions are evaluated at the nuclear radius R.

In 1982, the first description of the electron capture spectrum, which included only final states that involve a single hole in one of the core orbitals, was presented [90]. In 2014, the calculated spectrum from the same set of final states was improved by taking into account overlap and exchange corrections [91]. Since satellite structures were observed in the experimental spectrum [92], the calculations were extended for the consideration of two- [93, 94] and three-hole [95] excitations in dysprosium. It was demonstrated that two-hole states cannot be omitted and that three-hole states have a negligible impact on the spectral shape. A subject of interest was also shake-off processes [96], where, during atomic relaxation after electron capture, electrons are scattered into unbound states, leaving an ionized atom behind. An important question to answer was to what extent multi-core-hole states influence the spectral line shape at the end point, i.e., near $Q = 2833$ eV. Theoretical studies demonstrated that, although there are many two-core-hole states, there is no strong state near the end-point region. However, none of the calculations was able to explain the observed N1 (4s) satellite structure. Recently, this problem was solved in *ab initio* calculations of the calorimetric electron-capture spectrum by identifying it as an Auger peak [97].

Currently, three large experiments are being planned for the precise calorimetric measurement of the ^{163}Ho electron capture spectrum: ECHo [98], HOLMES [99], and Nu-MECS [100]. Large arrays of very high energy resolution detectors ($\Delta E_{\mathrm{FWHM}} < 3$ eV) will be employed in these experiments in order to acquire enough events to be sensitive to deviation in the spectral shape at the end-point region due to neutrinos with sub-eV mass.

4. Neutrinoless double beta decay

A distinctive signature of the Majorana nature of neutrino masses is the violation of lepton number by two units ($|\Delta L| = 2$), which manifests itself in neutrinoless double-beta decay (0νββ-decay) [101, 102],

$$(A, Z) \to (A, Z + 2) + 2\mathrm{e}^- , \quad (48)$$

and other processes like nuclear muon-to-positron conversion, or rare meson decays such as $\mathrm{K}^+ \to \pi^- \mathrm{e}^+ \mathrm{e}^+$, oscillations of neutrinos into antineutrinos, etc. However, 0νββ-decay is by far the most sensitive laboratory probe of total lepton number violation.

The experimental search for 0νββ-decay is based on the detection and exact measurement of the sum of the kinetic energies of two emitted electrons. Since the energy of the recoiling nucleus is negligible, the sum of the kinetic energies of both leptons must be equal to the Q-value of the transition. The signature is a monochromatic peak in the energy spectrum.

The search for 0νββ-decay represents a new frontier of neutrino physics. The experimental effort is concentrated on high $Q_{\beta\beta}$ isotopes, since this corresponds to a higher decay probability. The list of isotopes commonly under study includes ^{48}Ca, ^{76}Ge, ^{82}Se, ^{96}Zr, ^{100}Mo, ^{116}Cd, ^{130}Te, ^{136}Xe, and ^{150}Nd. But, progress is defined mostly by detector technology, not by the choice of isotope [103, 104].

0νββ-decay has not yet been observed. Table 2 shows the best results for today of the search for 0νββ-decay for the most interesting nucleus candidates for this process. Limits on the values of $T_{1/2}^{0\nu-\mathrm{exp}}$ and parameters $m_{\beta\beta}$ and $\eta_{\nu\mathrm{N}}$ of lepton-number violation are given. One can see that the best modern experiments, KamLAND-Zen [105] and EXO [106] (^{136}Xe), CUORE [107] (^{130}Te), and GERDA [108] and Majorana [109] (^{76}Ge), have reached a sensitivity of $\sim 10^{25} - 10^{26}$ years for the half-life.

The next generation of 0νββ-decay experiments requires more mass and a further reduction of backgrounds to maximize the discovery potential. A discovery potential is expected to be a half-life beyond 10^{28} years. For this half-life, an average signal rate of 1 decay per year requires tonnes of isotopes and precise techniques for detecting rare signals from emitted electrons with the exact determination of their energy. We are now entering the era of 0νββ-decay searches on a scale of tonnes [103, 104]. Many next-generation 0νββ-decay experiments are in preparation or under consideration, in particular the LEGEND (^{76}Ge, germanium detector technology) [118], SuperNEMO (^{82}Se, tracking plus calorimetry) [119], CUPID (^{100}Mo, scintillating bolometric experiment) [120, 121], AMoRE-II (^{100}Mo, crystal scintillators using a cryogenic detection technique) [122], SNO+II (^{130}Te, tellurium dissolved in liquid scintillator) [123], nEXO (^{136}Xe, liquid-xenon time projection chamber) [124], KamLAND2-Zen (^{136}Xe, xenon loaded liquid scintillator detector) [125], NEXT (^{136}Xe, high pressure xenon gas time projection chamber) [126], and PandaX-III (^{136}Xe, high pressure xenon time projection chamber) [127] experiments. They will be realized in $\sim 5-15$ years. Recall that KamLAND-Zen (^{136}Xe) [105] and CUORE (^{130}Te, bolometer) [107] are the first 0νββ-decay experiments on the scale of tonnes. Most of these projects follow an approach in stages in which the target mass is progressively increased.

The observation of 0νββ-decay will have important consequences: (i) it will signal that the lepton number is not conserved and neutrinos are Majorana particles; (ii) it represents the best hope for determining the absolute neutrino mass scale at the level of a few tens of meV. To achieve these goals, particle, nuclear, and experimental physics problems have to be overcome. Particle physics is important, since it provides the mechanisms for 0νββ-decay [128]. Nuclear physics is important for extracting the useful information from the data. To this end, it is necessary to accurately evaluate the relevant nuclear matrix elements, a formidable task [129].

In this review, the neutrino mass mechanisms of the 0νββ-decay are emphasized.

4.1 Light neutrino mass mechanism

The smallness of the neutrino masses suggests that they have a different origin with respect to other SM particles. The seesaw

Table 2. Upper bounds on the effective lepton number-violating parameters $m_{\beta\beta}$ and $\eta_{\nu N}$ imposed by current constraints on the 0νββ-decay half-life $T_{1/2}^{0\nu-\exp}$ (first row). Ranges of the LNV parameters were obtained using the largest and lowest values of $C_{\nu N}$ for a given isotope from Table 3, respectively. Unquenched value of the axial-vector coupling constant g_A is assumed.

	^{48}Ca	^{76}Ge	^{82}Se	^{100}Mo	^{116}Cd	^{130}Te	^{136}Xe	^{150}Nd
$T_{1/2}^{0\nu-\exp}$, years	5.6×10^{22}	1.8×10^{26}	3.5×10^{24}	1.5×10^{24}	2.2×10^{23}	3.2×10^{25}	1.07×10^{26}	2.0×10^{22}
Reference	[110]	[108]	[111]	[112, 113]	[114–116]	[107]	[105]	[117]
$m_{\beta\beta}$, eV	3.1–10	0.08–0.17	0.32–0.66	0.32–0.53	1.0–1.7	0.10–0.26	0.06–0.16	6.7–14
$\eta_{\nu N}\times10^6$	6.1–20	0.16–0.35	0.62–1.3	0.62–1.0	1.9–3.3	0.19–0.52	0.12–0.31	3.4–7.4

Table 3. Parameter $C_{\nu N}$ of the 0νββ-decay half-life for isotopes of experimental interest. Values are presented for nuclear matrix element $M_\nu^{0\nu}$ calculated within the interacting shell model (ISM) (Strasbourg–Madrid (StMa) [142] and Central Michigan University (CMU) [143] groups), interacting boson model (IBM) [144], quasiparticle random phase approximation (QRPA) (Tuebingen–Bratislava–Caltech (TBC) [145, 146] and Jyväskyla (Jy) [147] groups), projected Hartree–Fock–Bogoliubov approach (PHFB) [148], and covariant density functional theory (CDFT) [149] are considered. Argonne, CD-Bonn, and UCOM two-nucleon short-range correlations are taken into account. Unquenched value of the weak axial-vector coupling g_A is assumed.

Method	g_A	Short-range correlations	$C_{\nu N}$ (10^{-14} years^{-1})											
			^{48}Ca	^{76}Ge	^{82}Se	^{96}Zr	^{100}Mo	^{110}Pd	^{116}Cd	^{124}Sn	^{128}Te	^{130}Te	^{136}Xe	^{150}Nd
ISM-StMa	1.25	UCOM	4.38	4.56	17.3					15.1		24.4	17.1	
ISM-CMU	1.27	Argonne CD-Bonn	4.12 4.98	6.96 7.81	26.8 30.3					9.38 10.8		11.8 13.7	10.0 11.7	
IBM	1.27	Argonne	19.7	13.4	36.7	42.7	73.5	20.5	41.6	23.9	2.56	50.5	35.2	27.0
QRPA-TBC	1.27	Argonne CD-Bonn	1.88 2.24	16.3 19.0	56.7 66.4	39.5 46.8	120 141	41.4 48.9	70.7 81.6	15.4 19.9	3.17 3.93	55.8 70.4	18.0 22.9	
QRPA-Jy	1.26	CD-Bonn		16.5	35.6	51.1	61.0	51.6	76.4	64.0	3.59	57.3	31.1	
PHFB	1.25	Argonne CD-Bonn				40.5 44.6	132 143	59.6 64.7			2.18 2.39	50.4 55.0		23.7 25.6
CDFT	1.25	Argonne	47.3	22.4	74.0	216	173		128	42.3		88.2	68.0	113

I generation of tiny Majorana neutrino masses for the three observable very light neutrinos requires a very large Majorana mass term of right-handed neutrinos. In this case, along with very light neutrinos, very heavy Majorana neutrino mass states with typical masses of $\sim 10^{12}$ GeV also appear, and their contribution to 0νββ-decay can be safely neglected. Then, the conventional light neutrino exchange mechanism generated by left-handed $V-A$ weak currents is the dominant mechanism of 0νββ-decay. The inverse half-life of 0νββ-decay takes the form [102]

$$\left[T_{1/2}^{0\nu}\right]^{-1} = C_{\nu N}\left(\frac{m_{\beta\beta}}{m_e}\right)^2 \tag{49}$$

with

$$C_{\nu N} = G^{0\nu}(g_A^{\text{eff}})^4\left|M_\nu^{0\nu}(g_A^{\text{eff}})\right|^2. \tag{50}$$

Here, $G^{0\nu}$, g_A^{eff}, and $M^{0\nu}$ stand for the known phase-space factor [130, 131], the effective axial-vector coupling constant, and the nuclear matrix element (NME) of the process, respectively, and m_e is the mass of the electron.

The ultimate goal of the search for 0νββ-decay is to determine the Majorana neutrino mass $m_{\beta\beta}$. To deduce the value of $m_{\beta\beta}$ from a nonzero 0νββ-decay rate measurement, $M_\nu^{0\nu}$ and g_A^{eff} have to be reliably calculated using the tools of nuclear structure theory. The current most stringent limits on the effective mass of Majorana neutrinos $m_{\beta\beta}$ are obtained in experiments with ^{136}Xe, ^{130}Te, ^{76}Ge, ^{100}Mo, and ^{82}Se (see Table 2). The spread in the values of $m_{\beta\beta}$ is related to the currently existing uncertainties in the calculations of NMEs. The unquenched value of the axial vector coupling constant is assumed ($g_A^{\text{eff}} = g_A = 1.269$).

It was noted in Section 2.2 that $m_{\beta\beta}$ can be evaluated using neutrino oscillation parameters by making an assumption about the mass of the lightest neutrino and by choosing a type of spectrum (normal or inverted) and values of CP-violating Majorana phases. In future experiments, a sensitivity to $m_{\beta\beta}$ of a few tens of meV is planned to be reached. This is the region of the inverted hierarchy of neutrino masses ($m_{\beta\beta} = 19-50$ meV; see Fig. 2). If we are dealing with a normal spectrum, then everything depends on the value of $m_{\beta\beta}$ that is realized in nature. At $m_{\beta\beta} = 10-30$ meV, this lies in the sensitivity region of next-generation experiments, and 0νββ-decay could be registered. If $m_{\beta\beta} = 10$ meV, more sensitive experiments with 1–10 tons of ββ isotope are required, which might be feasible. For $m_{\beta\beta} = 1-3$ meV, experiments with 10–100 tons of the isotope are needed, and it will be very difficult to reach the required sensitivity in this case. If, however, $m_{\beta\beta}$ is below 3 meV, then apparently 0νββ-decay will not be registered in the foreseeable future.

In Fig. 6, predicted lifetimes of 0νββ-decay, obtained with $m_{\beta\beta} = 50$ meV (upper boundary for inverted hierarchy) and 3 meV (limit of any foreseeable experiment with current technologies) are displayed for isotopes of experimental interest. The range of values reflects the spread of calculated nuclear matrix elements for a given nucleus. The calculated half-lives are compared with the best current experimental limits on the 0νββ-decay half-life. In the case of ^{136}Xe, the current constraint is close to the range corresponding to the inverted hierarchy of neutrino masses.

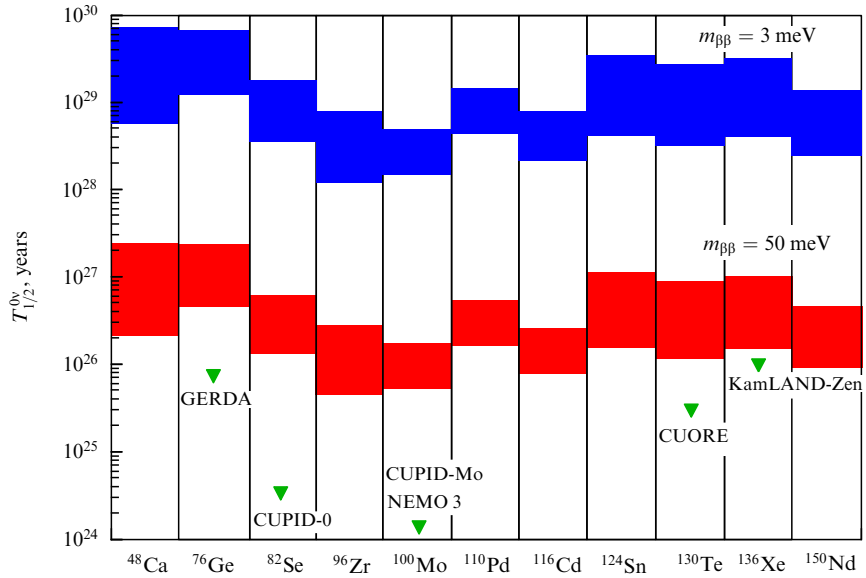

Figure 6. (Color online.) Values of 0νββ-decay half-lives of nuclei of experimental interest calculated for $m_{\beta\beta} = 3$ meV (blue region) and $m_{\beta\beta} = 50$ meV (red region). Upper and lower bounds of presented bands correspond to lowest and highest values of $C_{\nu N}$ coefficient in Table 3, i.e., width of the band reflects spread of calculated nuclear matrix elements for a given isotope. Current experimental constraints on the 0νββ-decay half-life are shown by filled green triangles. Unquenched value of weak-axial coupling constant g_A is assumed.

4.2 0νββ-decay with single heavy neutrino

Sterile right-handed neutrinos, which do not participate in the electroweak interactions, are natural candidates for the extension of the SM field contents.

In the case of active-sterile neutrino mixing, neutrino state ν_N with arbitrary mass m_N may appear. The neutrino mass eigenstate ν_N dominated by the sterile ν_s neutrino weak eigenstate contains some admixture of active $\nu_{e,\mu,\tau}$ neutrino species, as

$$\nu_N = \sum_{\alpha=s,e,\mu,\tau} U_{N\alpha}\nu_\alpha\,, \tag{51}$$

allowing ν_N to contribute to various processes, in particular to those with lepton flavor and lepton number violation.

The phenomenology of intermediate mass sterile neutrinos ν_N in various LNV processes has been actively studied in the literature (for a recent review, c.f. [132–135]) and limits in the $|U_{\alpha N}|^2 - m_N$-plane have been derived. It has been shown that 0νββ-decay limits for $|U_{eN}|^2 - m_N$ are the most stringent when compared with the limits from other LNV processes, except for a narrow region of this parametric plane [133, 136–138].

The contribution of the Majorana neutrino state, N, to the 0νββ-decay amplitude is described by the standard neutrino exchange diagram between the two β-decaying neutrons. Assuming the dominance of this LNV mechanism, the 0νββ-decay half-life for a transition to the ground state of the final nucleus takes the form

$$\left[T^{0\nu}_{1/2}\right]^{-1} = G^{0\nu}(g_A^{\rm eff})^4 \left|U^2_{eN} m_N\right|^2 \left|m_p\, M^{0\nu}(m_N, g_A^{\rm eff})\right|^2 . \tag{52}$$

The proton mass is denoted by m_p. The phase-space factor $G^{0\nu}$ is tabulated for various 0νββ-decaying nuclei in Refs [130, 131]. In the above formula, g_A and $g_A^{\rm eff}$ stand for the standard and 'quenched' values of the nucleon axial-vector coupling constant, respectively. Their meaning will be discussed in what follows. The nuclear matrix element in question $M^{0\nu}$ is given by

$$M^{0\nu}(m_N, g_A^{\rm eff}) = \frac{1}{m_p m_e}\frac{R}{2\pi^2 (g_A^{\rm eff})^2} \times \sum_n \int d^3x\, d^3y\, d^3p\, \exp\left[i\mathbf{p}(\mathbf{x}-\mathbf{y})\right] \times \frac{\langle 0_f^+|J_\mu^\dagger(\mathbf{x})|n\rangle\langle n|J_\mu^\dagger(\mathbf{y})|0_i^+\rangle}{\sqrt{p^2+m_N^2}\left(\sqrt{p^2+m_N^2}+E_n-(E_i-E_f)/2\right)}\,. \tag{53}$$

Here, R and m_e are the nuclear radius and the mass of electron, respectively. Initial and final nuclear ground states with energies E_i and E_f are denoted by $|0_i^+\rangle$ and $|0_f^+\rangle$, respectively. The summation runs over intermediate nuclear states $|n\rangle$ with energies E_n. The dependence on $g_A^{\rm eff}$ occurs in $M^{0\nu}$ through the weak one-body nuclear charged current $J_\mu^\dagger(x)$ [138].

For the two conventional limiting cases of the light $m_N \ll p_F$ and the heavy $m_N \gg p_F$ Majorana neutrino exchange mechanisms, where $p_F \sim 200$ MeV is the characteristic momentum transferred via the virtual neutrino, we have

$$M^{0\nu}(m_N \to 0, g_A^{\rm eff}) = \frac{1}{m_p m_e} M^{0\nu}_\nu(g_A^{\rm eff})\,, \tag{54}$$

$$M^{0\nu}(m_N \to \infty, g_A^{\rm eff}) = \frac{1}{m_N^2} M^{0\nu}_N(g_A^{\rm eff})\,. \tag{55}$$

The explicit form of NMEs associated with the exchange of very light and very heavy neutrinos will be given in Section 4.5.

For an arbitrary neutrino mass m_N, the half-life given in Eqn (52) is very inconvenient for use in practice. Fortunately, there is a very good approximate analytical representation

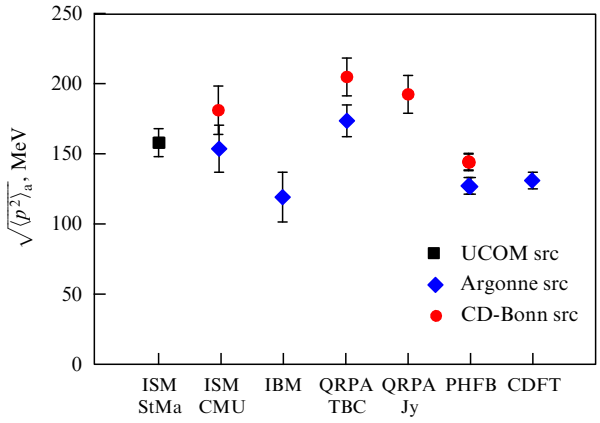

Figure 7. Average value $\sqrt{\langle p^2\rangle_a}$ over the set of considered isotopes with variance σ calculated within different nuclear structure approaches: interacting shell model (ISM) (Strasbourg–Madrid (StMa) [142] and Central Michigan University (CMU) [143] groups), interacting boson model (IBM) [144], quasiparticle random phase approximation (QRPA) (Tuebingen–Bratislava–Caltech (TBC) [145, 146] and Jyväskyla (Jy) [147] groups), projected Hartree–Fock–Bogoliubov approach (PHFB) [148], and covariant density functional theory (CDFT) [149]. The Argonne, CD-Bonn, and UCOM two-nucleon short-range correlations (src) are taken into account. The unquenched value of weak axial-vector coupling g_A is assumed.

with an 'interpolating formula' [138, 139],

$$\left[T_{1/2}^{0\nu}\right]^{-1} = C_{\nu N}\left|U_{eN}^2\,\frac{\langle p^2\rangle}{\langle p^2\rangle + m_N^2}\,\frac{m_N}{m_e}\right|^2, \tag{56}$$

where

$$\langle p^2\rangle = m_p m_e\,\frac{M_N^{0\nu}(g_A^{\rm eff})}{M_\nu^{0\nu}(g_A^{\rm eff})}\,, \tag{57}$$

which interpolates two limiting cases $m_N \ll p_F$ and $m_N \gg p_F$. It can be used for any value of m_N [133, 137, 140].

The form of Eqn (56) suggests the interpretation of $\langle p^2\rangle$ as the mean square momentum of the virtual neutrino propagating between two β-decaying nucleons. Therefore, it is expected to be of the order of $\langle p_F^2\rangle \sim (200\ \text{MeV})^2$. The values of $\sqrt{\langle p^2\rangle}$ calculated in different nuclear structure approaches for various isotopes together with its averaged value $\sqrt{\langle p^2\rangle_a}$ with variance σ are given in [141]. It was found that $\sqrt{\langle p^2\rangle}$ depends noticeably on the chosen nuclear structure method and considered choice of two-nucleon short-range correlation function. The values of $\sqrt{\langle p^2\rangle_a}$ are shown for different nuclear structure approaches and types of two-nucleon short-range correlations in Fig. 7. Surprisingly, within all the considered nuclear structure approaches, variance σ is very small, i.e., $\langle p^2\rangle$ is practically the same for all isotopes of experimental interest and can be replaced with averaged value $\langle p^2\rangle_a$.

Current constraints on the active-sterile mixing strength $|U_{eN}|^2$ in the regime $1\ \text{eV} < m_N < 10\ \text{TeV}$ derived from numerous experiments are summarized in Fig. 8 [150]. From accelerator experiments, the most stringent limits are in the range $1 < m_N < 100$ GeV. The constraints from astrophysics are important for $m_N \sim 10$ keV, where the heavy neutrino is a hot dark matter candidate. The spectra of electrons emitted in β-decays allows probing the heavy neutrino mass in the range $10\ \text{eV} < m_N < 1$ MeV. The current lower bounds on the 0νββ-decay half-life put stringent limits on $|U_{eN}|^2$ in the whole range of m_N if the heavy neutrino is a Majorana fermion.

4.3 Neutrino mass mechanisms of 0νββ-decay within left-right symmetric models

Left-right symmetric (LRS) models extend the SM gauge symmetry to the group $SU(2)_L \otimes SU(2)_R \otimes U(1)_{B-L}$ with an additional neutral Z' and two charged vector bosons $W_R^{\pm}$ [152, 153]. This symmetry group is broken down spontaneously into the SM group at a sufficiently high energy scale Λ_{LR}, providing large masses of $\sim \Lambda_{LR}$ to the extra gauge bosons Z', $W_R^{\pm}$. After integrating out these heavy particles, one ends up at low energies with the well-known current-current effective Lagrangian involving both left- and right-handed weak currents. The part which can trigger 0νββ-decay is

$$\mathcal{L}^{\beta} = \frac{G_\beta}{\sqrt{2}}\left[j_L^\rho J_{L\rho}^\dagger + \lambda j_R^\rho J_{R\rho}^\dagger + \text{H.c.}\right]. \tag{58}$$

Here, $\lambda = M_{W_L}/M_{W_R}$ (M_{W_L} and M_{W_R} are the masses of the light and heavy vector bosons, respectively). λ depends on the underlying high-scale model. The left-handed ν_{eL} and right-handed ν_{eR} weak eigenstate electron neutrinos are expressed as superpositions of the light and heavy mass eigenstate Majorana neutrinos ν_j and N_j as follows:

$$\begin{aligned}\nu_{eL} &= \sum_{j=1}^{3}\left(U_{ej}\nu_j + S_{ej}N_j^C\right),\\ \nu_{eR} &= \sum_{j=1}^{3}\left(T_{ej}^*\nu_j^C + V_{ej}^*N_j\right).\end{aligned} \tag{59}$$

The 3×3 block matrices in flavor space U, S, T, V form a 6×6 unitary neutrino mixing matrix, which diagonalizes the general 6×6 Dirac–Majorana neutrino mass matrix in the Lagrangian. Within the LRS models, small neutrino masses naturally arise within the see-saw mechanism. As a result, one ends up with 3 light m_i $(i = 1, 2, 3)$ and 3 heavy M_i $(i = 1, 2, 3)$ neutrino masses.

If only light and heavy Majorana neutrino mass mechanisms of 0νββ-decay are considered, the inverse 0νββ-decay half-life expressed with the 'interpolating formula' takes the form [154]

$$\left[T_{1/2}^{0\nu}\right]^{-1} = C_{\nu N}\left(\frac{m_{\beta\beta}^{\nu N}}{m_e}\right)^2, \tag{60}$$

where the effective Majorana neutrino mass for light and heavy neutrinos $m_{\beta\beta}^{\nu N}$ is given by

$$\begin{aligned}\left(m_{\beta\beta}^{\nu N}\right)^2 &= \left|\sum_{j=1}^{3}\left(U_{ej}^2 m_j + S_{ej}^2\,\frac{\langle p^2\rangle}{\langle p^2\rangle + M_j^2}\,M_j\right)\right|^2\\ &+ \lambda^2\left|\sum_{j=1}^{3}\left(T_{ej}^2 m_j + V_{ej}^2\,\frac{\langle p^2\rangle}{\langle p^2\rangle + M_j^2}\,M_j\right)\right|^2.\end{aligned} \tag{61}$$

From Eqns (60) and (61), it follows that the dominance of light or heavy neutrino mechanisms of the 0νββ-decay cannot be established by observing this process in different isotopes. This task requires additional information or assumptions concerning neutrino masses and mixing.

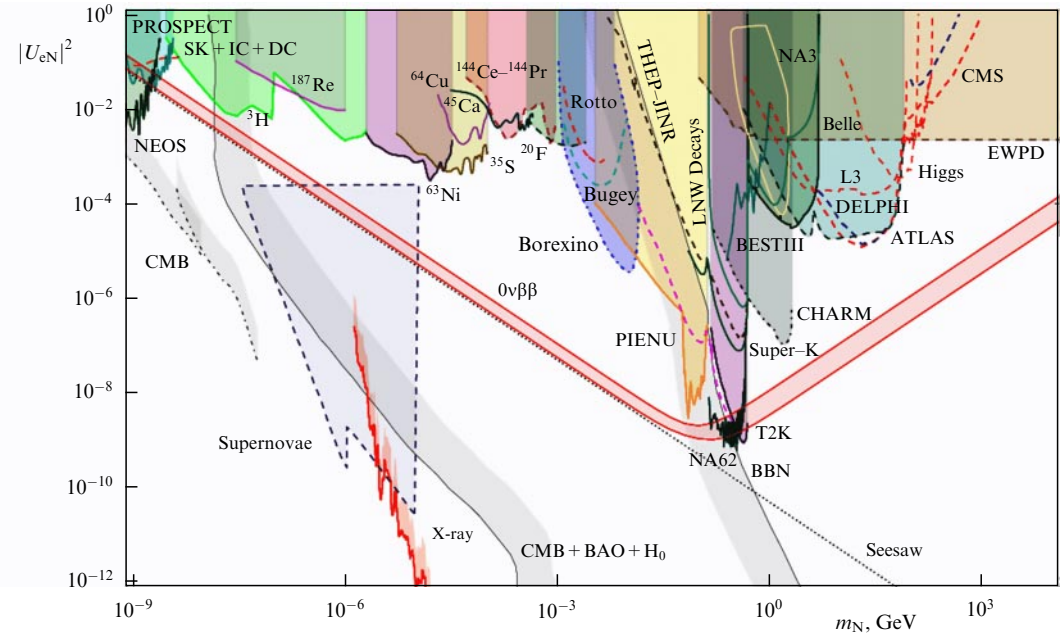

Figure 8. Exclusion plots in the $|U_{eN}|^2 - m_N$ plane [150]. For simplicity, ν_e is assumed to be the only active neutrino. Shaded regions are excluded by searches and observations as labeled (c.f. [151]). Band labeled '0νββ' denotes the uncertainty about the current upper limit from 0νββ-decay searches for a Majorana heavy neutrino ν_N. Diagonal black dotted line labeled 'Seesaw' indicates the standard seesaw relation $|U_{eN}|^2 = m_{\nu_e}/m_N$ with $m_{\nu_e} = 0.05$ eV.

If the universality of mixing between the active and sterile neutrino sectors is assumed, the seesaw mixing matrix $\mathcal{U}$ takes the form [154]

$$\mathcal{U} = \begin{pmatrix} U & S \\ T & V \end{pmatrix} \simeq \frac{1}{\sqrt{1+\zeta^2}} \begin{pmatrix} U & \zeta\,\mathbb{1} \\ -\zeta\,\mathbb{1} & U^\dagger \end{pmatrix}. \tag{62}$$

Here, $\zeta \ll 1$ is the seesaw parameter ($1 + \zeta^2 \simeq 1$), and U and $U^\dagger$ are the PMNS neutrino mixing matrix and its Hermitian conjugate, respectively.

In order to reach a conclusion about the possible importance of the $m_{\beta\beta}$ and $M^R_{\beta\beta}$ mechanisms, the see-saw relation $m_i \simeq \zeta^2 M_i$ ($m_i \neq 0$ and $\zeta \ll 1$) for light and heavy neutrino masses is assumed. If the LNV scale is significantly larger than $\langle p^2 \rangle_a$, we have

$$\left(m^{\nu N}_{\beta\beta}\right)^2 = m^2_{\beta\beta} + \left(M^R_{\beta\beta}\right)^2, \tag{63}$$

with

$$\begin{aligned} m_{\beta\beta} &= \left| \sum_j^3 \left(U^2_{ej} + \frac{\zeta^4 \langle p^2 \rangle_a}{\zeta^4 \langle p^2 \rangle_a + m_j^2} \right) m_j \right|, \\ M^R_{\beta\beta} &= \frac{\lambda}{\zeta^2} \left| \sum_j^3 \left(\zeta^4 + (U^\dagger_{ej})^2 \, \frac{\zeta^4 \langle p^2 \rangle_a}{\zeta^4 \langle p^2 \rangle_a + m_j^2} \right) m_j \right|. \end{aligned} \tag{64}$$

We note that $m_{\beta\beta}$ ($M^R_{\beta\beta}$) depends on θ_{12}, θ_{13}, α_1, α_2 (θ_{12}, θ_{13}, θ_{23}, δ), $m_{1,2,3}$, and ζ. These quantities can be evaluated by making assumptions about the normal spectrum ($m_1 < m_2 < m_3$) or inverted spectrum ($m_3 < m_1 < m_2$) of neutrino masses and considering CP violating phases to be arbitrary.

The current constraint on the mass of W_R, $M_{W_R} \geqslant 2.9$ TeV [155], sets the limit $\lambda \leqslant 7.7 \times 10^{-4}$. The upper limit $\lambda = 7.7 \times 10^{-4}$ will be used as a reference value for this parameter. In Fig. 9, the region of dominance of the $M^R_{\beta\beta}$ mechanism over the $m_{\beta\beta}$ mechanism in the 0νββ-decay rate

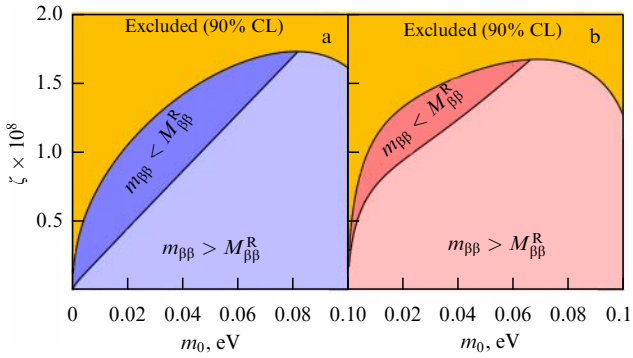

Figure 9. Region of the dominance of $M^R_{\beta\beta}$ contribution over $m_{\beta\beta}$ contribution to $m^{\nu N}_{\beta\beta}$ for the seesaw type of neutrino mixing matrix given in Eqn (18) and by assuming $\zeta^2 \simeq m_i/M_i$. Cases of normal and inverted hierarchy of neutrino masses are presented in the left and right panels, respectively. Current constraint on the $\eta_{\nu N}$ parameter is deduced from the lower limit on the 0νββ-decay half-life of ^{136}Xe [105] by using nuclear matrix element calculated within the quasiparticle random phase approximation (QRPA) [145].

is displayed in the plane of parameters ζ and m_0 (the lightest neutrino mass). The cases of normal (a) and inverted (b) mass spectra of neutrino masses are presented. The upper limit on the 0νββ-decay half-life $T^{0\nu-exp}_{1/2}(^{136}\text{Xe}) > 1.07 \times 10^{26}$ is considered [105]. It is found that for $m_0 \gtrsim 0.8$ eV the light neutrino exchange mechanism ($m_{\beta\beta}$) dominates over the one related to heavy neutrino exchange ($M^R_{\beta\beta}$). For a lower value of m_0, there is a region governed by the $M^R_{\beta\beta}$ mechanism, in spite of its significant suppression due to the smallness of λ.

4.4 Quark condensate seesaw in 0νββ-decay

Let us discuss 0νββ-decay in the context of the dimension-7 operator $\mathcal{O}^u_7$ in Eqn (3). After the EWSB, this operator generates $\Delta L = 2$ effective interactions relevant to 0νββ-

decay. We have [28]

$$\mathcal{L}_7 = \frac{G_F}{\sqrt{2}}\,\varepsilon_{ee}\left(\overline{e_L}\,\nu_L^C\,\overline{u_R}\,d_L + \overline{\nu_L^C}\,\nu_L\overline{u_R}\,u_L\right) + \text{H.c.}\,, \tag{65}$$

$$\varepsilon_{\alpha\beta} = \frac{g_{\alpha\beta}\,v/\Lambda^3}{G_F}\,. \tag{66}$$

Here, $\varepsilon_{\alpha\beta}$ is a measure of the relative strength of the four-fermion interactions with respect to the Fermi constant G_F.

The first term in Eqn (65) combined with the SM weak charged-current interaction leads to the contribution shown in Fig. 10b, which is independent of neutrino mass in the propagator due to chiralities in the vertices $P_L\,(m_\nu + \not{q})\,P_R = \not{q}$. This is a manifestation of the fact that $\Delta L = 2$ is not provided by m_ν, but solely by the upper vertex in Fig. 10b. In the considered QCSS model, the second term in (65) also contributes to 0νββ-decay via the neutrino-mass mechanism shown in Fig. 10a. This happens due to chiral symmetry breaking and the formation of a quark condensate. As we discussed in previous sections, this term is the only source of neutrino mass in the present model. We note that neutrino mass is generated in the nuclear environment, where the chiral quark condensate $\langle\overline{q}q\rangle_N$ is suppressed with respect to the one in a vacuum $\langle\overline{q}q\rangle$.

The inverse 0νββ-decay half-life in the QCSS model can be written as [28]

$$\left(T_{1/2}^{0\nu}\right)^{-1} = |\varepsilon_{ee}|^2\left|1 + a_\nu\,f_{nme}\right|^2 (g_A^{eff})^2\,|M_\epsilon^{0\nu}|^2\,G^{0\nu}\,, \tag{67}$$

where

$$f_{nme} = g_A^{eff}\,\frac{M_\nu^{0\nu}}{M_\epsilon^{0\nu}}\,. \tag{68}$$

Nuclear matrix elements M_ν and M_ϵ are associated with mechanisms in Fig. 10a and b, respectively. Their explicit form is given in [28]. By exploiting the prediction of the QCSS model, we have

$$a_\nu = \frac{m_{\beta\beta}}{\varepsilon_{ee}m_e} = \frac{\langle\overline{q}q\rangle_N}{\sqrt{2}\,m_e}\,G_F = -1.83\times10^{-4}\,. \tag{69}$$

Here, $\langle\overline{q}q\rangle_N$ is the value of quark condensate in the nuclear environment of a decaying nucleus, which is different from the vacuum value $\langle\overline{q}q\rangle$. For the 0νββ-decay of ^{136}Xe, $a_\nu f_{nme} \simeq -2.00\times10^{-7}$ within the QRPA approach. Recall that contributions to the 0νββ-decay amplitude of the diagrams in Fig. 10 are proportional to the first and second terms in vertical brackets in Eqn (67), respectively. Thus, due to the smallness of $a_\nu f_{nme}$, the diagram in Fig. 10b clearly dominates in the considered scenario.

From what is currently the most stringent upper bound on the 0νββ-decay half-life obtained for ^{136}Xe by the KamLAND-Zen experiment ($T_{1/2}^{0\nu-exp} > 1.07\times10^{26}$ years [105]), the upper bounds on LNV parameters are as follows:

$$|\varepsilon_{ee}| < 2.49\times10^{-10}\,,\quad |m_{\beta\beta}| < 2.33\times10^{-5}\ \text{meV}\,. \tag{70}$$

It is worth recalling that in the QCSS $m_{\beta\beta}$ characterizes the subdominant contribution to the 0νββ decay shown in Fig. 10a, while the dominant one is given by the diagram Fig. 10b.

Comparing the limit for $m_{\beta\beta}$ in (70) with the allowed region for this quantity in Fig. 2, derived from neutrino-oscillation data, it is concluded that the QCSS predicts the normal ordering of neutrino masses and a rather narrow interval of the lightest neutrino mass [28]:

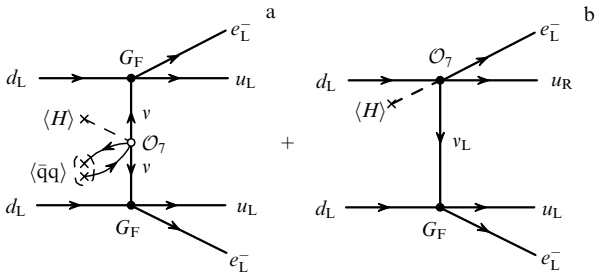

Figure 10. Contributions of effective operators (3) to 0νββ-decay.

$$2.65 < m_0 = m_1 < 6.84\ \text{meV}\,. \tag{71}$$

Using the 1σ ranges of the neutrino-oscillation parameters $\sin^2\theta_{ij}$ and Δm_{ij}^2 from Ref. [156], narrow ranges for masses of the other two neutrino masses are obtained:

$$9.0 < m_2 < 11.2\ \text{meV}\,, \tag{72}$$

$$49.8 < m_3 < 50.8\ \text{meV}\,. \tag{73}$$

From limits (71)–(73), the corresponding range for the cosmological neutrino parameter is as follows:

$$61.4 < \Sigma = \sum_i m_i < 68.8\ \text{meV}\,. \tag{74}$$

The QCSS range for the single-beta-decay parameter,

$$9.0 < m_\beta = \sqrt{\sum_i |U_{ei}|^2\,m_i^2} < 11.4\ \text{meV}\,, \tag{75}$$

is beyond the reach of current tritium beta-decay experiments and those in the near future (see, for instance, [39, 71]).

4.5 0νββ-decay nuclear matrix elements

Nuclear matrix elements for 0νββ-decay must be evaluated using nuclear structure methods. There are no observables that could be directly related to the magnitude of 0νββ nuclear matrix elements and that could be used to determine them in a model independent way.

The nuclear matrix elements $M_\nu^{0\nu}$ and $M_N^{0\nu}$ associated with the exchange of light (sub-eV scale) and heavy (TeV scale) neutrinos, respectively, consists of Fermi, Gamow–Teller, and tensor parts as

$$M_{\nu,N}^{0\nu}(g_A^{eff}) = -\frac{M_F^{(\nu,N)}}{(g_A^{eff})^2} + M_{GT}^{(\nu,N)}(g_A^{eff}) + M_T^{(\nu,N)}(g_A^{eff})$$
$$= \langle 0_i^+|\sum_{kl}\tau_k^+\tau_l^+\left[-\frac{H_F(r_{kl})}{(g_A^{eff})^2} + H_{GT}(r_{kl})\sigma_{kl} - H_T(r_{kl})S_{kl}\right]|0_f^+\rangle \tag{76}$$

with

$$\mathbf{r}_{12} = \mathbf{r}_1 - \mathbf{r}_2\,,\quad r_{12} = |\mathbf{r}_{12}|\,,\quad \hat{\mathbf{r}}_{12} = \frac{\mathbf{r}_{12}}{r_{12}}\,,$$
$$\sigma_{12} = \boldsymbol{\sigma}_1\,\boldsymbol{\sigma}_2\,,\quad S_{12} = 3(\boldsymbol{\sigma}_1\,\hat{\mathbf{r}}_{12})(\boldsymbol{\sigma}_2\,\hat{\mathbf{r}}_{12}) - \sigma_{12}\,. \tag{77}$$

Here, $\mathbf{r}_1$ and $\mathbf{r}_2$ are the coordinates of the nucleons undergoing beta decay.

The radial parts of the exchange neutrino potentials are integrals over the exchanged momentum q,

$$H_K^{(\nu,\mathrm{N})}(r_{12}, E_{J^\pi}^k) = \frac{2}{\pi} R \int_0^\infty f_K(qr_{12}) F^{(\nu,\mathrm{N})}(q^2)\, h_K(q^2) q^2 \,\mathrm{d}q\,. \tag{78}$$

The functions $f_{\mathrm{F,GT}}(qr_{12}) = j_0(qr_{12})$ and $f_{\mathrm{T}}(qr_{12}) = -j_2(qr_{12})$ are spherical Bessel functions. The functions $h_K(q^2)$ that enter the H_K's through the integrals over q have the form

$$h_{\mathrm{F}}(q^2) = g_{\mathrm{V}}^2(q^2)\,, \tag{79}$$

$$h_{\mathrm{GT}}(q^2) = \frac{g_{\mathrm{A}}^2(q^2)}{g_{\mathrm{A}}^2}\left[1 - \frac{2}{3}\frac{q^2}{q^2+m_\pi^2} + \frac{1}{3}\left(\frac{q^2}{q^2+m_\pi^2}\right)^2\right] + \frac{2}{3}\frac{g_{\mathrm{M}}^2(q^2)}{(g_{\mathrm{A}}^{\mathrm{eff}})^2}\frac{q^2}{4m_{\mathrm{p}}^2}\,,$$

$$h_{\mathrm{T}}(q^2) = \frac{g_{\mathrm{A}}^2(q^2)}{g_{\mathrm{A}}^2}\left[\frac{2}{3}\frac{q^2}{q^2+m_\pi^2} - \frac{1}{3}\left(\frac{q^2}{q^2+m_\pi^2}\right)^2\right] + \frac{1}{3}\frac{g_{\mathrm{M}}^2(q^2)}{(g_{\mathrm{A}}^{\mathrm{eff}})^2}\frac{q^2}{4m_{\mathrm{p}}^2}\,. \tag{80}$$

Here, the partially conserved axial current (PCAC) hypothesis has been employed. The finite nucleon size is taken into account via momentum dependence of the nucleon form-factors. For the vector, weak-magnetism, and axial-vector form factors, the usual dipole approximations are adopted:

$$g_{\mathrm{V}}(q^2) = \frac{g_{\mathrm{V}}}{(1+q^2/M_{\mathrm{V}}^2)^2}\,,$$

$$g_{\mathrm{M}}(q^2) = (\mu_{\mathrm{p}} - \mu_{\mathrm{n}}) g_{\mathrm{V}}(q^2)\,, \tag{81}$$

$$g_{\mathrm{A}}(q^2) = \frac{g_{\mathrm{A}}^{\mathrm{eff}}}{(1+q^2/M_{\mathrm{A}}^2)^2}\,,$$

where $g_{\mathrm{V}} = 1$, $\mu_{\mathrm{p}} - \mu_{\mathrm{n}} = 3.70$. The parameters $M_{\mathrm{V}} = 850$ MeV and $M_{\mathrm{A}} = 1086$ MeV come from electron scattering and neutrino charged-current scattering experiments.

The difference between the calculations of $M_\nu^{0\nu}(g_{\mathrm{A}}^{\mathrm{eff}})$ and $M_{\mathrm{N}}^{0\nu}(g_{\mathrm{A}}^{\mathrm{eff}})$ has its origin in factors $F^{(\nu,\mathrm{N})}(q^2)$. We have

$$F^{(\nu)}(q^2) = \frac{1}{q(q+\bar{E})}\,, \quad F^{(\nu,\mathrm{N})}(q^2) = \frac{1}{m_{\mathrm{e}} m_{\mathrm{p}}}\,. \tag{82}$$

Here, $\bar{E}$ is the average of the virtual intermediate nuclear states used in the closure approximation.

Significant progress has been achieved in the last decade in the evaluation of matrix elements $M_\nu^{0\nu}$ and $M_{\mathrm{N}}^{0\nu}$ for $0\nu\beta\beta$-decay [129]. Nevertheless, there is still a spread by a factor of 2–3 between the $M_\nu^{0\nu}$ calculations using different nuclear models. While earlier evaluations of NMEs were performed mostly within the quasiparticle random phase approximation (QRPA) and interacting shell model (ISM), nowadays, the results of the interacting boson model (IBM) and of different versions of the energy density functional (EDF) are also available. It is generally accepted that all these models are plagued by neglecting certain essential aspects of physics, different in each case. Currently, it is difficult, or impossible, to reliably assign the corresponding uncertainties in the resulting NMEs. For these nuclear model-based

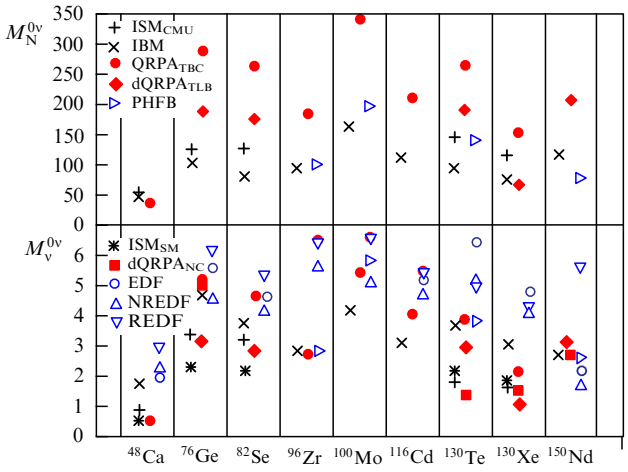

Figure 11. (Color online.) Nuclear matrix elements $M_\nu^{0\nu}$ and $M_{\mathrm{N}}^{0\nu}$ for $0\nu\beta\beta$-decay candidates calculated in the framework of different approaches: (i) interacting shell model (Strasbourg–Madrid (ISM$_{\mathrm{SM}}$, [142]) and Central Michigan University (ISM$_{\mathrm{CMU}}$, [143]) groups) and interacting boson model (IBM, [144]) in black; (ii) spherical (Tuebingen–Bratislava–Caltech (QRPA$_{\mathrm{TBC}}$, [145]) group) and deformed (Tuebingen–Lanzhou–Bratislava (dQRPA$_{\mathrm{TLB}}$, [159]) and North Carolina (dQRPA$_{\mathrm{NC}}$, [160]) groups) quasiparticle random phase approximation in red; (iii) projected Hartree–Fock–Bogoliubov (PHFB, [161]), nonrelativistic energy density functional (EDF, [162]) and (NREDF, [163]) and Relativistic EDF (REDF, [164]) methods in blue. In the case of ISM$_{\mathrm{CMU}}$, IBM, QRPA$_{\mathrm{TBC}}$, dQRPA$_{\mathrm{TLB}}$, and PHFB [161] calculations, Argonne two-nucleon short-range correlations (src) were considered. ISM$_{\mathrm{SM}}$ results are with Jastrow src. Effect of src was neglected in dQRPA$_{\mathrm{NC}}$, EDF, NREDF, and REDF evaluation of NMEs. Unquenched value of weak axial-vector coupling g_{A} and $R = 1.2$ fm $A^{1/3}$ are assumed.

methods, the concrete issues that are widely discussed are the role of ground state correlations, deformation, the size of the model space, or the restoration of the SU(4) spin-isospin symmetry [157, 158]. The approaches with 'controlled errors,' like the no core shell model, coupled cluster methods, or the Green's function Monte Carlo method, are being developed. They are, however, so far applicable only to light nuclear systems and not yet to relatively heavy $0\nu\beta\beta$-decay candidate nuclei.

In Fig. 11, $M_\nu^{0\nu}$ and $M_{\mathrm{N}}^{0\nu}$ calculated within different nuclear structure methods are presented. We notice that the ISM results are significantly smaller when compared with results of different mean field approaches (PHFB, EDF, NREDF, and REDF). The importance of the relative deformation of initial and final nuclei in evaluating NMEs is manifested by a difference between results of spherical and deformed QRPA.

It is assumed that the problem of reliable calculation of $0\nu\beta\beta$-decay NMEs can be resolved with the help of supporting nuclear structure experiments. An example is the study of the heavy-ion double-charge exchange reaction (with $\Delta T = 2$), in particular of ground state to ground state transitions, at LNC Catania (the NUMEN experiment [165, 166]). This and the analogous low energy pion double charge exchange reaction are potentially related to the NME of $0\nu\beta\beta$-decay. That relation, however, requires further theoretical study [167].

4.6 Relation between $0\nu\beta\beta$- and $2\nu\beta\beta$-decay NMEs

For any mechanism responsible for decay, the matrix element $M^{0\nu}$ consists of three parts, Fermi (F), Gamow–Teller (GT),

and Tensor (T):

$$M^{0\nu} = M^{0\nu}_{\rm GT} - \frac{M^{0\nu}_{\rm F}}{(g^{\rm eff}_{\rm A})^2} + M^{0\nu}_{\rm T}\,. \tag{83}$$

By considering the closure approximation, we have

$$\left\{ \begin{array}{c} M^{0\nu}_{\rm F} \\ M^{0\nu}_{\rm GT} \\ M^{0\nu}_{\rm T} \end{array} \right\} = \langle f| \sum_{j,k}^{A} \tau_j^+ \tau_k^+ \left\{ \begin{array}{c} P_{\rm F}(r_{jk}) \\ P_{\rm GT}(r_{jk})\sigma_{jk} \\ P_{\rm T}(r_{jk}) S_{jk} \end{array} \right\} |i\rangle \tag{84}$$

with

$$\sigma_{jk} = \boldsymbol{\sigma}_j\,\boldsymbol{\sigma}_k\,, \quad S_{ij} = 3(\boldsymbol{\sigma}_j\,\hat{\mathbf{r}}_{jk})(\boldsymbol{\sigma}_k\,\hat{\mathbf{r}}_{jk}) - \boldsymbol{\sigma}_j\,\boldsymbol{\sigma}_k\,. \tag{85}$$

Here, $|i\rangle$ and $|f\rangle$ are the ground state wave functions of the initial and final nuclei, and $P_{\rm GT}(r_{jk})$, $P_{\rm F}(r_{jk})$, and $P_{\rm T}(r_{jk})$ are the potentials that depend on the relative distance r_{jk} of the two nucleons. The sum is over all nucleons in the nucleus.

For the light and heavy neutrino mass mechanisms, the dimensionless neutrino potential for the $K = {\rm GT}$, F, and T parts are

$$\left\{ \begin{array}{c} P^{\nu}_K(r_{jk}) \\ P^{\rm N}_K(r_{jk}) \end{array} \right\} = f^2_{\rm src}(r_{jk}) \times \frac{2}{\pi g^2_{\rm A}}\, R \int_0^{\infty} f_K(qr_{jk})\, h_K(q^2) \left(\begin{array}{c} \dfrac{1}{q(q+E_{\rm av})} \\ \dfrac{1}{m_{\rm e} m_{\rm p}} \end{array} \right) q^2\, {\rm d}q\,. \tag{86}$$

Here, R is the nuclear radius added to make the potential dimensionless. The functions $f_{\rm F,\,GT}(qr_{jk}) = j_0(qr_{jk})$ and $f_{\rm T}(qr_{jk}) = -j_2(qr_{jk})$ are spherical Bessel functions. The functions $h_K(q^2)$ are defined in [157]. The light neutrino exchange potential depends rather weakly on average nuclear excitation energy $E_{\rm av}$. The function $f_{\rm src}(r_{jk})$ represents the effect of two-nucleon short range correlations [168].

Better insight into the structure of matrix elements can be gained by explicitly considering their dependence on the distance r between the two neutrons that are transformed into two protons in the decay. Thus we define the function $C^{0\nu}_{\rm GT}(r)$ (and analogous ones for $M_{\rm F}$ and $M_{\rm T}$) as

$$C^{0\nu-\nu,\,{\rm N}}_{\rm GT}(r) = \langle f| \sum_{j,k} \tau_j^+ \tau_k^+ \boldsymbol{\sigma}_j\,\boldsymbol{\sigma}_k\, \delta(r - r_{jk}) P^{\nu,\,{\rm N}}_{\rm GT}(r_{jk})|i\rangle\,,$$

$$\text{i.e.,}\quad M^{0\nu-\nu,\,{\rm N}}_{\rm GT} = \int_0^{\infty} C^{0\nu-\nu,\,{\rm N}}_{\rm GT}(r)\,{\rm d}r\,. \tag{87}$$

In other words, knowledge of $C^{0\nu-\nu,\,{\rm N}}_{\rm GT}(r)$ makes the evaluation of $M^{0\nu-\nu,\,{\rm N}}_{\rm GT}$ trivial. We note that the function $C(r)$ was first introduced in [157].

From the way the function $C^{0\nu-\nu,\,{\rm N}}_{\rm GT}(r)$ was constructed, it immediate follows that

$$\begin{aligned} C^{0\nu-\nu,\,{\rm N}}_{\rm GT}(r) &= P^{\nu,\,{\rm N}}_{\rm GT}(r)\, C^{2\nu}_{\rm GT\,cl}(r)\,, \\ C^{2\nu}_{\rm GT\,cl}(r) &= \langle f| \sum_{j,k} \tau_j^+ \tau_k^+ \boldsymbol{\sigma}_j\,\boldsymbol{\sigma}_k\, \delta(r - r_{jk})|i\rangle\,, \end{aligned} \tag{88}$$

as already pointed out in [169]. $C^{2\nu}_{\rm GT\,cl}(r)$ determines the two-neutrino double-beta decay closure matrix element $M^{2\nu}_{\rm GT\,cl}$ as a result of integration over r. From (88), it follows that, if $C^{2\nu}_{\rm GT\,cl}(r)$ is known, the $C^{0\nu-\nu,\,{\rm N}}_{\rm GT}(r)$ can be easily constructed and hence also the $0\nu\beta\beta$-decay matrix element $M^{0\nu-\nu,\,{\rm N}}_{\rm GT}$. The analogous procedure can also be followed, of course, for

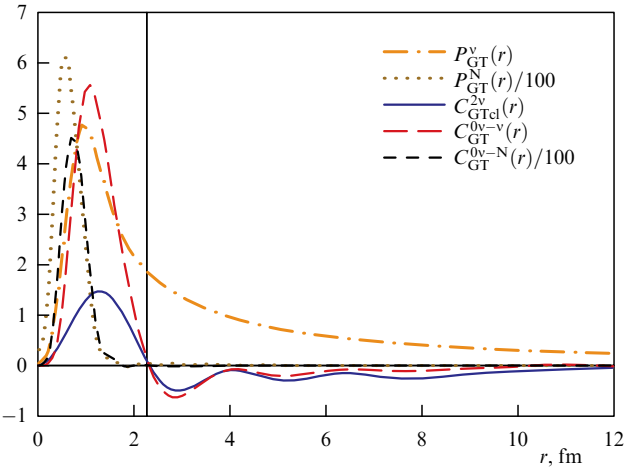

Figure 12. Neutrino exchange potentials $P^{\nu}_{\rm GT}(r)$, $P^{\rm N}_{\rm GT}(r)$ and functions $C^{2\nu}_{\rm GT\,cl}(r)$, $C^{0\nu-\nu,\,{\rm N}}_{\rm GT}(r)$ $(C^{0\nu-\nu,\,{\rm N}}_{\rm GT}(r) = P^{\nu,\,{\rm N}}_{\rm GT}(r) C^{2\nu}_{\rm GT\,cl}(r))$ evaluated in the QRPA [145] for the $0\nu\beta\beta$-decay of ^{76}Ge.

$M^{0\nu-\nu,\,{\rm N}}_{\rm F}$ and $M^{0\nu-\nu,\,{\rm N}}_{\rm T}$. But Eqn (88) is much more general. Knowing $C^{2\nu}_{\rm GT\,cl}(r)$ makes it possible to evaluate the corresponding matrix element for any neutrino potential $P^{0\nu}_{\rm GT}(r)$. That represents, no doubt, a significant practical simplification. A better understanding of the $C^{2\nu}_{\rm GT\,cl}(r)$ function is a key to a reliable calculation of double beta decay NMEs [158].

For the $0\nu\beta\beta$-decay of ^{76}Ge, the functions $C^{0\nu-\nu,\,{\rm N}}_{\rm GT}(r)$ and $C^{2\nu}_{\rm GT\,cl}(r)$ calculated within the QRPA [145] and related neutrino exchange potential $P^{\nu,\,{\rm N}}_{\rm GT}(r)$ are displayed in Fig. 12, where $C^{0\nu-\nu,\,{\rm N}}_{\rm GT}(r)$ refers to two curves, $C^{0\nu-\nu}_{\rm GT}(r)$ and $C^{0\nu-{\rm N}}_{\rm GT}(r)$. These functions are defined by the relation

$$C^{0\nu-\nu,\,{\rm N}}_{\rm GT}(r) = P^{\nu,\,{\rm N}}_{\rm GT}(r) C^{2\nu}_{\rm GT\,cl}(r)\,,$$

where $P^{\nu,\,{\rm N}}_{\rm GT}(r)$ denotes $P^{\nu}_{\rm GT}(r)$ and $P^{\rm N}_{\rm GT}(r)$ (see also Eqn (88)).

4.7 Quenching of axial-vector coupling constant

The value of the axial-vector coupling constant at the quark level is unity and for a free nucleon is larger, namely $g_{\rm A} = 1.269$, as strong interaction renormalizes the weak axial-vector current for neutron decay. What its value is in the case of a bound nucleon in a nucleus has not been solved yet. It is well known that the calculated strengths of Gamow–Teller beta-decay nuclear transitions to individual final states are significantly larger than the experimental ones. That effect is known as axial-vector current matrix elements quenching. To account for this, it is customary to quench the calculated GT matrix elements [170–172]. Formally, this is accomplished by replacing the true value of the coupling constant $g_{\rm A} = 1.269$ by a quenched, value $g^{\rm eff}_{\rm A} < g_{\rm A}$. There is no consensus on the origin of quenching of $g_{\rm A}$. It could be missing correlations in the nuclear wave functions, or single-particle model truncation, or the renormalization of the Gamow–Teller operator, including the inclusion of two-body currents. This effect might also be assigned to the delta-isobar admixture in the nuclear wave function or to the shift of GT strength to higher excitation energies due to short-range tensor correlations. It is not known yet whether a similar phenomenon exists for other multipoles, besides $J = 1^+$.

The renormalized or quenched value of axial-vector coupling constant $g^{\rm eff}_{\rm A}$, which includes nuclear medium effects, is the important source of uncertainty in the theor-

etical predictions of the 0νββ-decay half-life and is a major concern in experiments looking for a sign of 0νββ-decay. It should be borne in mind that $g_A^{\rm eff}$ enters in the fourth power in both the 0νββ- and 2νββ-decay rates. Different nuclear methods (e.g., nuclear shell model, interacting boson model, and QRPA) can be used to compute 2νββ-decay lifetimes. The predicted lifetimes for these processes are almost always shorter than the measured lifetimes, i.e., computed 2νββ NMEs are too large. The problems are usually solved by using $g_A^{\rm eff}$ in place of the bare value of $g_A = 1.269$ for a free nucleon.

There are some indications that the value of $g_A^{\rm eff}$ can be significantly suppressed when compared to g_A. First, by QRPA statistical analyses that took into account experimental EC and β rates, in addition to the measured 2νββ-decay half-lives, it was found that $(g_A^{\rm eff})^4 = 0.30$ and 0.50 for the 2νββ-decay of ^{100}Mo and ^{116}Cd, respectively [171]. This kind of study was extended for a number of isobaric triplets and more complicated isobaric chains of nuclei in [173, 174]. The striking result of Ref. [171] was confirmed by a conclusion that $g_A^{\rm eff} \leqslant 0.80$. Second, a significantly stronger quenching of the axial-vector coupling constant, namely, $(g_A^{\rm eff})^4 \simeq (1.269A^{-0.18})^4 = 0.063$, was established within the interacting boson model by exploiting the 2νββ-decay matrix elements evaluated within the closure approximation [172].

The problem of quenching of the axial-vector coupling constant may be related to a partial restoration of the spin-isospin SU(4) symmetry within the QRPA [158]. This restoration of symmetry was achieved by using a new way of adjusting the isoscalar particle-particle interaction of the residual Hamiltonian in the way the matrix element of the double Gamow–Teller operator connecting the initial and final ground states of double-beta decay vanishes. The obtained values of $M_\nu^{0\nu}$ were found to be not very different ($\leqslant 20\%$) from the usual QRPA values when isoscalar particle-particle interaction is related to known 2νββ half-lives. Figure 13 shows a comparison of the NMEs produced by both ways of renormalization of this interaction. By assuming partial restoration of the SU(4) symmetry, the true 2νββ-decay matrix elements were evaluated and compared to the corresponding experimental values. It was found that calculated values are mostly larger than the experimental ones, suggesting qualitatively, on average, a relatively modest quenching, $g_A^{\rm eff} = 0.90$ [158].

Recently, by combining effective field theories (EFTs) of the strong and weak forces with powerful quantum many-body techniques, state-of-the-art computations of β-decays from light- and medium-mass nuclei have been presented [175]. EFTs enable a consistent description of the coupling of weak interactions to two nucleons via two-body currents. The three-nucleon forces make smaller but significant corrections to the nuclear interaction, and in a standard treatment of single β and double-beta decay processes are not usually taken into account.

In calculations with consistent nuclear Hamiltonians and two-body currents, where the two-body current operators are transformed into effective one-body operators, matrix elements of single-β and 2νββ-decay are reduced by an amount corresponding to $g_A^{\rm eff} = (0.7-0.8)g_A$ [175, 176]. Thus, the puzzle of the quenching of axial-vector coupling constant seems to be largely solved. In the case of calculation of 0νββ-decay NMEs with two-body currents, the effect at high momentum transfer, which softens the quenching, has to be taken into account. The corresponding reduction in NMEs

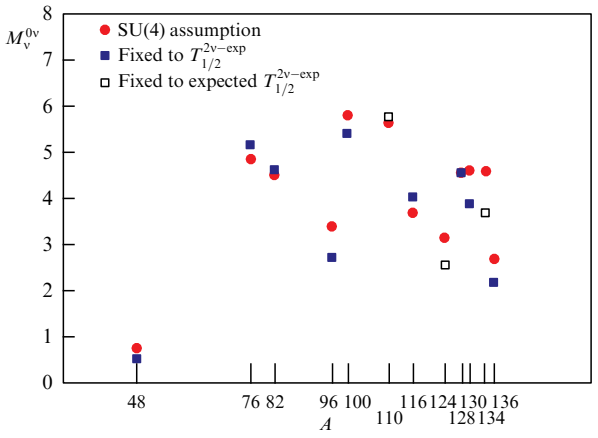

Figure 13. (Color online.) Nuclear matrix elements ($M_\nu^{0\nu}$) for 0νββ-decay candidates as a function of mass number A. Results are taken from the QRPA [158]. Isoscalar particle–particle interaction is adjusted by a partial restoration of the SU(4) symmetry (red dots) and 2νββ-decay experimental half-life is correctly reproduced (blue squares). Where the 2νββ-decay half-life is not measured (^{94}Zr, ^{110}Pd, ^{124}Sn, and ^{134}Xe), the expected 2νββ-decay half-life, e.g., within the single-state dominance hypothesis, is considered (unfilled black squares). $g_A^{\rm eff} = g_A^{\rm free} = 1.269$ is assumed.

turns out to be about 30% and 20% within the nuclear shell model [176] and QRPA [177], respectively. It is much less than would be obtained by squaring the renormalization factor from single-β decay, as one does to get the quenching of 2νββ matrix elements.

The quenching phenomenon has been firmly established for low momentum transfer GT-type nuclear transitions. However, the 0νββ involves momentum transfer $q \sim 100$ MeV, with no restriction on angular momentum and parity change. This makes the muon capture with relatively large momentum transfer of the order of the muon mass and unrestrictive selection rules an important testing ground for a nuclear model description of 0νββ-decay NMEs. Recently, there is some experimental (see, e.g., Ref. [178] and references therein) and theoretical [179, 180] effort in this direction.

There seems to be a discrepancy between the calculated muon capture rates based on the QRPA method in the older Refs [181–183], where only mild quenching of g_A was required, and more recent Ref. [179], where rather substantial quenching is indicated. Recently, a detailed calculation of the total muon capture rates for final nuclei participating in double-beta decay was performed within the QRPA [180]. Several variants of the muon capture formalism were considered. The analysis included a different size of the single particle model space used or the treatment of the initial bound muon wave function. The experimental total capture rates are compared with the calculated rates for $g_A^{\rm eff} = 1.27$ and 1.0 in Fig. 14. Clearly, the experimental data are bracketed by these two $g_A^{\rm eff}$ values. Thus, it is not necessary to significantly reduce the axial current coupling constant g_A. Its standard value $g_A = 1.27$ seems to be adequate.

5. Two-neutrino double beta decay

Two-neutrino double beta decay (2νββ-decay) [101],

$$(A, Z) \to (A, Z+2) + 2e^- + 2\bar{\nu}_e\,, \tag{89}$$

is a second order process of weak interaction fully consistent with the Standard Model of particle physics, where two

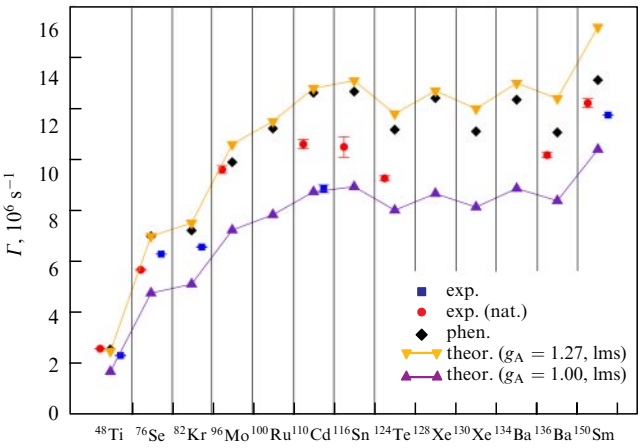

Figure 14. (Color online.) Comparison of experimental and theoretical total capture rates for the final nuclei participating in double-beta decay. Measurements were performed for a given isotope in [178] and for elements with a natural abundance of isotopes. Theoretical results were obtained within QRPA with large model space (lms) for $g_A = 1.00$ and 1.27.

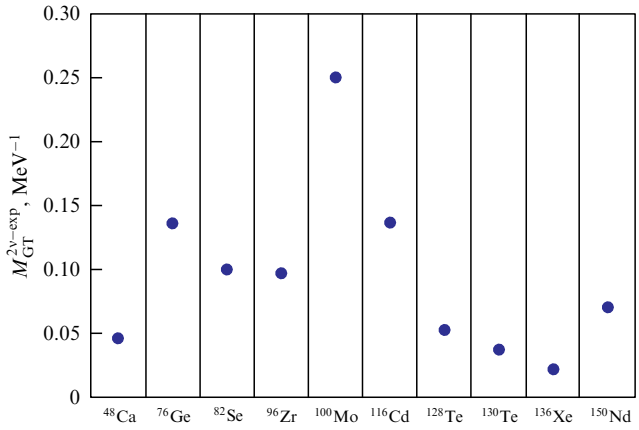

Figure 15. 2νββ-decay matrix elements deduced from measured half-lives. Unquenched value of axial-vector coupling constant is assumed.

protons are simultaneously transformed into two neutrons inside an atomic nucleus, and two pairs of electrons and antineutrinos are emitted.

2νββ-decay has been a subject of experimental research for more than 60 years. The first direct observation of this process dates back to 1987 [184]. Currently, 2νββ-decay has been observed in eleven even-even nuclei with a transition to the ground state and in two cases also with a transition to the first excited 0_1^+ state of the final nucleus [185]. It is the rarest process measured so far in nature with a half-life above 10^{18} years and a source of background in experiments looking for signs of 0νββ-decay.

The inverse half-life of 2νββ-decay is commonly presented by the product of a phase-space factor $G^{2\nu}$, fourth power of the effective axial-vector coupling constant $g_A^{\rm eff}$, and nuclear matrix element $M_{\rm GT}^{2\nu}$ as follows:

$$\left(T_{1/2}^{2\nu}\right)^{-1} = (g_A^{\rm eff})^4 |M_{\rm GT}^{2\nu}|^2 G^{2\nu}. \tag{90}$$

The nuclear matrix element expressed in terms of sequential single β-decay Gamow–Teller transitions through complete set of virtual intermediate states is given by

$$M_{\rm GT}^{2\nu} = \sum_n \frac{\langle 0_f^+ \| \sum_{k=1}^A \tau_k^+ \boldsymbol{\sigma}_k \| 1_n^+ \rangle \langle 1_n^+ \| \sum_{k=1}^A \tau_k^+ \boldsymbol{\sigma}_k \| 0_i^+ \rangle}{E_n - (E_i + E_f)/2}. \tag{91}$$

Here, $|0_i^+\rangle$ ($|0_f^+\rangle$) is the ground state of the initial (final) even-even nuclei with energy E_i (E_f), and $|1_n^+\rangle$ are the states in the intermediate odd-odd nucleus with energies E_n.

The matrix element $M_{\rm GT}^{2\nu}$, the value of which can be determined from the measured 2νββ half-life by making assumptions about the value of $g_A^{\rm eff}$ (Fig. 15), plays an important role in understanding the nuclear structure of double beta decay isotopes [186]. Its value is usually used to adjust the residual part of the nuclear Hamiltonian in calculating the 0νββ-decay NME within the proton-neutron quasiparticle random phase approximation (pn-QRPA) [187–189]. Due to this procedure, the results obtained are only weakly sensitive to the size of the model space and chosen type of nucleon–nucleon (NN) interaction. So far, 2νββ-decay NMEs have been calculated without the closure approximation only within the interacting shell model (ISM) [190] and the pn-QRPA [191].

There is a possibility of exploring new physics beyond the SM with 2νββ-decay by a precise measurement of the 2νββ-decay differential distributions. It covers the search for right-handed neutrino interactions without having to assume their nature [192], neutrino self-interactions [193], sterile neutrinos with masses up to the Q-value of the process [194], the bosonic neutrino component [195], violation of Lorentz invariance [196–199], 0νββ-decays with Majoron emission [200, 201], and quadruple-β-decay [202].

5.1 Improved description of 2νββ-decay

Experiments studying two-neutrino double-beta decay (2νββ-decay) are currently approaching a qualitatively new level, where high-precision measurements are performed not only for half-lives but for all other observables of the process. A reconstruction of individual electron energies allowed obtaining information about the single state dominance (SSD) and higher state dominance (HSD) hypotheses [203, 204], discussing the importance of various contributions to the 2νββ-decay NME from transitions through intermediate nuclear states [205, 206].

In this context, a more accurate expression for the 2νββ-decay half-life was derived by taking into account the dependence of energy denominators on lepton energies and using a Taylor expansion, which allows calculation of phase-space factors and NMEs to be factorized [207]:

$$\left(T_{1/2}^{2\nu}\right)^{-1} = (g_A^{\rm eff})^4 |M_{\rm GT-3}^{2\nu}|^2 \frac{1}{|\xi_{31}^{2\nu}|^2} \left(G_0^{2\nu} + \xi_{31}^{2\nu} G_2^{2\nu}\right), \tag{92}$$

where $G_0^{2\nu}$ and $G_2^{2\nu}$ are the phase-space factors with different dependences on lepton energies. The new parameter $\xi_{31}^{2\nu} = M_{\rm GT-3}^{2\nu}/M_{\rm GT}^{2\nu}$ depends on $M_{\rm GT-3}^{2\nu}$ and $M_{\rm GT}^{2\nu}$, NMEs with the first and third power of the energy denominators, respectively. While $M_{\rm GT}^{2\nu}$ is sensitive to contributions from high-lying states in the intermediate odd-odd nucleus with $J^\pi = 1^+$, for $M_{\rm GT-3}^{2\nu}$, typically only the lowest 1^+ state contributes. It was found that the value of an additional contribution to the 2νββ-decay width corresponds to 3–20% of the full width for $A = 76$, 81, 96, and 100 nuclear systems [207].

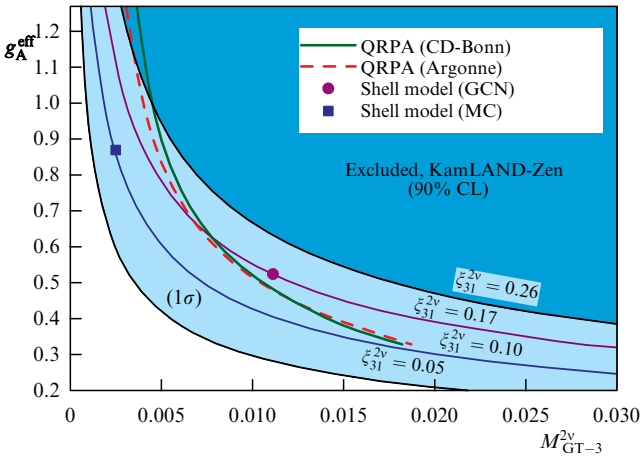

Figure 16. Effective axial-vector coupling constant g_A^{eff} versus matrix element $M^{2\nu}_{GT-3}$ for 2νββ-decay of ^{136}Xe [208]. Purple dot and blue square display ISM results with the CGN5082 and MC interactions, respectively. QRPA dependence is shown by the solid green and dashed red curves.

The improved description of 2νββ-decay made it possible to also introduce a novel approach for determining the effective axial-vector coupling constant. The revised expression for the 2νββ-decay half-life includes, in addition to the well-known nuclear matrix element $M^{2\nu}_{GT-1}$, the double Gamow–Teller matrix element $M^{2\nu}_{GT-3}$ with energy denominator to the third power. This matrix element is governed by the transitions through the lowest states of the intermediate nucleus. It was proposed that the effective axial-vector coupling constant g_A^{eff} can be determined from the measured 2νββ-decay half-life if the ratio $\xi^{2\nu}_{13}$ of nuclear matrix elements $M^{2\nu}_{GT-3}$ and $M^{2\nu}_{GT-1}$ is deduced phenomenologically from the shape of the energy spectrum of emitted electrons in the 2νββ-decay, and nuclear matrix element $M^{2\nu}_{GT-3}$ is reliably calculated, e.g., within the interacting shell model. In this way, one avoids the problem of the importance of transitions through the higher lying states of the intermediate nucleus.

By using 2νββ-decay data, $\xi^{2\nu}_{31}$ can be determined experimentally with electron energy spectrum fits extracting the leading and second order contributions in Eqn (92). This new observable $\xi^{2\nu}_{31}$ makes it possible to test and discriminate between QRPA and ISM calculations that all reproduce the experimental $T^{2\nu}_{1/2}$. In Fig. 16, the effective axial-vector coupling constant g_A^{eff} is displayed as a function of the matrix element M_{GT-3} for the 2νββ-decay of ^{136}Xe. It is shown that $\xi^{2\nu}_{31} > 0.26$ (0.05) is excluded by the present KamLAND-Zen measurement at 90% (1σ) CL [208]. Further experimental $\xi^{2\nu}_{31}$ sensitivity improvements may distinguish between various nuclear structure scenarios.

6. Conclusions and outlook

In recent years, we have witnessed a revolution in the physics of neutrinos. The observation of neutrino oscillations demonstrated both the mixing of neutrinos and that neutrinos are massive particles. There is a strong oscillation program, including a precise measurement of mixing angles, the search for CP violation in the neutrino sector, and a possibility of reaching a conclusion about the mass hierarchy of three neutrinos. But, neutrino oscillation measurements shed light neither on the scale of neutrino masses, nor on the mechanism by which they are generated.

Cosmology and single and double-beta decay processes can probe the absolute neutrino mass scale in complementary ways. The neutrino mass scale is most directly accessed by studying the energy spectrum generated by the β-decay of tritium in the KATRIN experiment with a technique proposed by Spivak and Lobashev [66] a long time ago. Also promising are studies of electron capture of ^{163}Ho with cryogenic calorimeters in the ECHo and Holmes experiments.

Searching for 0νββ-decay is a top priority in particle and astroparticle physics, being the most sensitive test of lepton number violation and the only suitable process to probe the Majorana nature of neutrinos. In order to increase the experimental sensitivity for this particular search, detectors on the scale of tonnes operated under nearly zero-background conditions with a few keV energy resolution are required. The race to observe 0νββ-decay has started. If there is an inverted hierarchy of neutrino masses, many of the 0νββ-decay experiments (SuperNEMO, CUORE, nEXO, LEGEND, AMoRE, CUPID, etc.) can establish the nature of neutrinos in the coming decade.

The possible existence of sterile neutrinos is an opportunity with many interesting phenomenological consequences and is a challenge for theory and experiment. Beta-decay experiments allow us, in theory, to reach a conclusion about additional heavy neutrinos in the eV (driven by the reactor neutrino anomaly), keV (hot dark matter candidate), and even MeV ranges. If neutrinos are Dirac particles, an important constraint on their masses and mixing can be deduced from differential characteristics of 2νββ-decay. In the opposite case, namely if neutrinos are Majorana particles, stringent constraints on the masses and mixing of sterile neutrinos are deduced from the upper bound on 0νββ-decay from various experiments.

To interpret the data from weak nuclear processes accurately, a better understanding of nuclear structure effects important for the description of nuclear matrix elements is needed. In this connection, it is crucial to develop theoretical methods capable of evaluating reliably the nuclear matrix elements and to realistically asses their uncertainties. As the field developed, the mysteries of neutrinos became more intriguing, theories more exciting, experiments more varied and larger, and the number of physicists involved larger. Many important discoveries are on the way.

In writing this review, the author would like to give credit to the Institute for Nuclear Research of the Russian Academy of Sciences (INR RAS), which recently celebrated 50 years since its foundation, for important and decisive contributions in the field of neutrino physics recognized worldwide, in particular, for the success of the Troitsk nu-Mass and KATRIN laboratory experiments used to measure the neutrino mass kinematically and the double-beta decay experiments GERDA and AMoRE. However, the research at the institute is much broader, covering the topics of neutrino theory, astrophysics, and cosmology. There is no doubt that the INR RAS will also achieve many important results and make more discoveries in the future.

Acknowledgments

This study was supported by the VEGA Grant Agency of the Slovak Republic under contract no. 1/0607/20 and by the Ministry of Education, Youth and Sports of the Czech Republic under the INAFYM grant no. CZ.02.1.01/0.0/0.0/16_019/0000766.

References

1. Fukuda Y et al. (Super-Kamiokande Collab.) *Phys. Rev. Lett.* **81** 1562 (1998)
2. Ahmad Q R et al. (SNO Collab.) *Phys. Rev. Lett.* **89** 011301 (2002)
3. Weinberg S *Phys. Rev. Lett.* **43** 1566 (1979)
4. Minkowski P *Phys. Lett. B* **67** 421 (1977)
5. Mohapatra R N, Senjanović G *Phys. Rev. Lett.* **44** 912 (1980)
6. Yanagida T *Conf. Proc. C* **7902131** 95 (1979)
7. Gell-Mann M, Ramond P, Slansky R *Conf. Proc. C* **790927** 315 (1979)
8. Magg M, Wetterich Ch *Phys. Lett. B* **94** 61 (1980)
9. Schechter J, Valle J W F *Phys. Rev. D* **22** 2227 (1980)
10. Wetterich C *Nucl. Phys. B* **187** 343 (1981)
11. Mohapatra R N, Senjanović G *Phys. Rev. D* **23** 165 (1981)
12. Cheng T P, Li L-F *Phys. Rev. D* **22** 2860 (1980)
13. Foot R et al. *Z. Phys. C* **44** 441 (1989)
14. Ma E *Phys. Rev. Lett.* **81** 1171 (1998)
15. Ma E, Roy D P *Nucl. Phys. B* **644** 290 (2002)
16. Bajc B, Senjanović G *J. High Energy Phys.* **2007** (08) 014 (2007)
17. Ma E, Popov O *Phys. Lett. B* **764** 142 (2017)
18. Yao C-Y, Ding G-J *Phys. Rev. D* **96** 095004 (2017)
19. Yao C-Y, Ding G-J *Phys. Rev. D* **98** 039901 (2018)
20. Centelles Chuliá S, Srivastava R, Valle J W F *Phys. Rev. D* **98** 035009 (2018)
21. Centelles Chuliá S et al. *J. High Energy Phys.* **2019** (10) 93 (2019)
22. Arbeláez C et al. *Phys. Rev. D* **100** 115021 (2019)
23. Arbeláez C et al. *J. High Energy Phys.* **2020** (06) 043 (2020)
24. Babu K S et al. *J. High Energy Phys.* **2020** (03) 006 (2020)
25. Bonnet F et al. *J. High Energy Phys.* **2009** (10) 076 (2009)
26. Babu K, Nandi S *Phys. Rev. D* **62** 033002 (2000)
27. Chen M-C, de Gouvêa A, Dobrescu B A *Phys. Rev. D* **75** 055009 (2007)
28. Babič A, Kovalenko S, Krivoruchenko M I, Šimkovic F *Phys. Rev. D* **103** 015007 (2021)
29. Päs H et al. *Phys. Lett. B* **453** 194 (1999)
30. Deppisch F F, Hirsch M, Päs H *J. Phys. G* **39** 124007 (2012)
31. Arbeláez C et al. *Phys. Rev. D* **94** 096014 (2016)
32. Arbeláez C et al. *Phys. Rev. D* **97** 099904 (2018)
33. Cirigliano V et al. *J. High Energy Phys.* **2017** (12) 082 (2017)
34. Thomas S D, Xu R-M *Phys. Lett. B* **284** 341 (1992)
35. McNeile C et al. *Phys. Rev. D* **87** 034503 (2013)
36. Capozzi F et al. *Phys. Rev. D* **101** 116013 (2020)
37. Aghanim N et al. (Planck Collab.) *Astron. Astrophys.* **641** A6 (2020)
38. Chacko Z et al. *J. High Energy Phys.* **2020** (04) 020 (2020)
39. Drexlin G et al. *Adv. High Energy Phys.* **2013** 293986 (2013)
40. Kovalenko S, Krivoruchenko M I, Šimkovic F *Phys. Rev. Lett.* **112** 142503 (2014)
41. Giunti C et al. *Phys. Rev. D* **86** 113014 (2012)
42. Aguilar A et al. (LSND Collab.) *Phys. Rev. D* **64** 112007 (2001)
43. Aguilar-Arevalo A A et al. (MiniBooNE Collab.) *Phys. Rev. Lett.* **121** 221801 (2018)
44. Serebrov A P et al. *JETP Lett.* **109** 213 (2019); *Pis'ma Zh. Eksp. Teor. Fiz.* **109** 209 (2019)
45. Hampel W et al. (GALLEX Collab.) *Phys. Lett. B* **420** 114 (1998)
46. Abdurashitov J et al. (SAGE Collab.) *Phys. Rev. C* **80** 015807 (2009)
47. Mention G et al. *Phys. Rev. D* **83** 073006 (2011)
48. Watson C R, Li Z, Polley N K *JCAP* **2012** (03) 018 (2012)
49. Boyarsky A et al. *Mon. Not. R. Astron. Soc.* **387** 1361 (2008)
50. Xing Z *Phys. Rev. D* **85** 013008 (2012)
51. Babič A, Kovalenko S, Krivoruchenko M I, Šimkovic F *Phys. Rev. D* **98** 015003 (2018)
52. Petcov S T *Phys. Lett. B* **110** 245 (1982)
53. Valle J W F *Phys. Rev. D* **27** 1672 (1983)
54. de Gouvêa A, Huang W-C, Jenkins J *Phys. Rev. D* **80** 073007 (2009)
55. Anamiati G, Fonseca R M, Hirsch M *Phys. Rev. D* **97** 095008 (2018)
56. Anamiati G et al. *Phys. Rev. D* **100** 035032 (2019)
57. Khatun A, Smetana A, Šimkovic F *Symmetry* **12** 1310 (2020)
58. Fermi E *Z. Phys.* **88** 161 (1934)
59. Alichanian A I, Alichanow A I, Dželepow B S *Phys. Rev.* **53** 766 (1938)
60. Šimkovic F, Dvornický R, Faessler A *Phys. Rev. C* **77** 055502 (2008)
61. Kim C W, Primakoff H *Phys. Rev.* **139** B1447 (1965)
62. Kim C W, Primakoff H *Phys. Rev.* **140** B566 (1965)
63. Kim C W *Phys. Rev.* **146** 691 (1966)
64. Hanna G C, Pontecorvo B *Phys. Rev.* **75** 983 (1949)
65. Bergkvist K-E *Nucl. Phys.* **39** 317 (1972)
66. Lobashev V M, Spivak P E *Nucl. Instrum. Meth. Phys. Res. A* **240** 305 (1985)
67. Picard A et al. *Nucl. Instrum. Meth. Phys. Res. B* **63** 345 (1992)
68. Lobashev V M *Nucl. Phys. A* **719** C153 (2003)
69. Aseev V N et al. *Phys. Rev. D* **84** 112003 (2011)
70. Kraus Ch et al. *Eur. Phys. J. C* **40** 447 (2005)
71. Aker M et al. (KATRIN Collab.) *Phys. Rev. Lett.* **123** 221802 (2019)
72. Asner D M et al. (Project 8 Collab.) *Phys. Rev. Lett.* **114** 162501 (2015)
73. Betts S et al., arXiv:1307.4738
74. Guigue M (Project 8 Collab.) *J. Phys. Conf. Ser.* **1342** 012025 (2020)
75. Belesev A I et al. *JETP Lett.* **97** 67 (2013); *Pis'ma Zh. Eksp. Teor. Fiz.* **97** 73 (2013)
76. Kraus Ch et al. *Eur. Phys. J. C* **73** 2323 (2013)
77. Aker M et al. (KATRIN Collab.) *Phys. Rev. Lett.* **126** 091803 (2021)
78. Abdurashitov J N et al. *JETP Lett.* **105** 753 (2017); *Pis'ma Zh. Eksp. Teor. Fiz.* **105** 723 (2017)
79. Watson C R, Li Z, Polley N K *JCAP* **2012** (03) 018 (2012)
80. Boyarsky A et al. *Prog. Part. Nucl. Phys.* **104** 1 (2019)
81. Brunst T *J. Phys. Conf. Ser.* **1468** 012195 (2020)
82. Mertens S et al. *J. Phys. G* **48** 015008 (2020)
83. Dvornický R, Muto K, Šimkovic F, Faessler A *Phys. Rev. C* **83** 045502 (2011)
84. Arnaboldi C et al. *Phys. Rev. Lett.* **96** 042503 (2006)
85. Doi M, Kotani T, Takasugi E *Prog. Theor. Phys. Suppl.* **83** 1 (1985)
86. Gatti F *Nucl. Phys. B Proc. Suppl.* **91** 293 (2001)
87. Sisti M et al. *Nucl. Instrum. Meth. Phys. Res. A* **520** 125 (2004)
88. Andreotti E et al. (MARE Collab.) *Nucl. Instrum. Meth. Phys. Res. A* **572** 208 (2007)
89. Eliseev S et al. *Phys. Rev. Lett.* **115** 062501 (2015)
90. De Rújula A, Lusignoli M *Phys. Lett. B* **118** 429 (1982)
91. Faessler A, Gastaldo L, Šimkovic F *J. Phys. G* **42** 015108 (2015)
92. Ranitzsch P C-O et al. *Phys. Rev. Lett.* **119** 122501 (2017)
93. Robertson R G H *Phys. Rev. C* **91** 035504 (2015)
94. Faessler A, Šimkovic F *Phys. Rev. C* **91** 045505 (2015)
95. Faessler A, Enss C, Gastaldo L, Šimkovic F *Phys. Rev. C* **91** 064302 (2015)
96. Faessler A, Gastaldo L, Šimkovic F *Phys. Rev. C* **95** 045502 (2017)
97. Braß M et al. *Phys. Rev. C* **97** 054620 (2018)
98. Gastaldo L et al. *Eur. Phys. J. Spec. Top.* **226** 1623 (2017)
99. Alpert B et al. *Eur. Phys. J. C* **75** 112 (2015)
100. Croce M P et al. *J. Low Temp. Phys.* **184** 938 (2016)
101. Vergados J D, Ejiri H, Šimkovic F *Rep. Prog. Phys.* **75** 106301 (2012)
102. Vergados J D, Ejiri H, Šimkovic F *Int. J. Mod. Phys. E* **25** 1630007 (2016)
103. Agostini M, Benato G, Detwiler J A *Phys. Rev. D* **96** 053001 (2017)
104. Barabash A S *Front. Phys.* **6** 160 (2019)
105. Gando A et al. (KamLAND-Zen Collab.) *Phys. Rev. Lett.* **117** 082503 (2016)
106. Anton G et al. (EXO Collab.) *Phys. Rev. Lett.* **123** 161802 (2019)
107. Adams D Q et al. (CUORE Collab.) *Phys. Rev. Lett.* **124** 122501 (2020)
108. Agostini M et al. (GERDA Collab.) *Phys. Rev. Lett.* **125** 252502 (2020)
109. Alvis S I et al. (Majorana Collab.) *Phys. Rev. C* **100** 025501 (2019)
110. Umehara S et al. *Phys. Rev. C* **78** 058501 (2008)
111. Azzolini O et al. *Phys. Rev. Lett.* **123** 032501 (2019)
112. Arnold R et al. (NEMO-3 Collab.) *Phys. Rev. D* **92** 072011 (2015)
113. Armengaud E et al. (CUPID-Mo Collab.) *Phys. Rev. Lett.* **126** 181802 (2021)
114. Danevich F A et al. *Nucl. Phys. B Proc. Suppl.* **138** 230 (2005)
115. Arnold R et al. (NEMO-3 Collab.) *Phys. Rev. D* **95** 012007 (2017)
116. Barabash A S et al. *Phys. Rev. D* **98** 092007 (2018)
117. Arnold R et al. (NEMO-3 Collab.) *Phys. Rev. D* **94** 072003 (2016)
118. Abgrall N et al. (LEGEND Collab.) *AIP Conf. Proc.* **1894** 020027 (2017)
119. Cascella M et al. (SuperNEMO Collab.) *J. Phys. Conf. Ser.* **888** 012249 (2017)

120. Wang G et al. (CUPID Interest Group), arXiv:1504.03599
121. Armstrong W R et al. (CUPID Interest Group), arXiv:1907.09376
122. Seo K (AMoRE Collab.) *J. Phys. Conf. Ser.* **1468** 012130 (2020)
123. Leming E J (SNO + Collab.) *PoS* **NOW2018** 027 (2019)
124. Albert J B et al. (nEXO Collab.) *Phys. Rev. C* **97** 065503 (2018)
125. Shirai J (KamLAND-Zen Collab.) *J. Phys. Conf. Ser.* **888** 012031 (2017)
126. Adams C et al. (NEXT), arXiv:2005.06467
127. Chen X et al. *Sci. China Phys. Mech. Astron.* **60** 061011 (2017)
128. Dell'Oro S et al. *Adv. High Energy Phys.* **2016** 2162659 (2016)
129. Engel J, Menéndez J *Rep. Prog. Phys.* **80** 046301 (2017)
130. Kotilla J, Iachello F *Phys. Rev. C* **85** 034316 (2012)
131. Mirea M, Rahomi T, Stoica S *Rom. Rep. Phys.* **67** 872 (2015)
132. Atre A et al. *J. High Energy Phys.* **2009** (05) 030 (2009)
133. Helo J C, Kovalenko S, Schmidt I *Nucl. Phys. B* **853** 80 (2011)
134. Abazajian K N et al., arXiv:1204.5379
135. Adhikari R et al. *JCAP* **2017** (01) 025 (2017)
136. Beneš P, Faessler A, Kovalenko S, Šimkovic F *Phys. Rev. D* **71** 077901 (2005)
137. Mitra M, Senjanović G, Vissani F *Nucl. Phys. B* **856** 26 (2012)
138. Faessler A, González M, Kovalenko S, Šimkovic F *Phys. Rev. D* **90** 096010 (2014)
139. Kovalenko S, Lu Z, Schmidt I *Phys. Rev. D* **80** 073014 (2009)
140. Abada A, De Romeri V, Teixeira A M *J. High Energy Phys.* **2014** (09) 074 (2014)
141. Babič A, Kovalenko S, Krivoruchenko M I, Šimkovic F *Phys. Rev. D* **98** 015003 (2018)
142. Menéndez J et al. *Nucl. Phys. A* **818** 139 (2009)
143. Horoi M, Neacsu A *Phys. Rev. C* **93** 024308 (2016)
144. Barea J, Kotila J, Iachello F *Phys. Rev. C* **91** 034304 (2015)
145. Šimkovic F et al. *Phys. Rev. C* **87** 045501 (2013)
146. Fang D-L, Faessler A, Šimkovic F *Phys. Rev. C* **92** 044301 (2015)
147. Hyvärinen J, Suhonen J *Phys. Rev. C* **91** 024613 (2015)
148. Rath P K et al. *Phys. Rev. C* **85** 014308 (2012)
149. Song L S et al. *Phys. Rev. C* **95** 024305 (2017)
150. Bolton P D, Deppisch F F, Gráf L, Šimkovic F *Phys. Rev. D* **103** 055019 (2021)
151. Bolton P D, Deppisch F F, Bhupal Dev P S *J. High Energy Phys.* **2020** (03) 170 (2020)
152. Pati J C, Salam A *Phys. Rev. D* **10** 275 (1974)
153. Mohapatra R, Pati J C *Phys. Rev. D* **11** 2558 (1975)
154. Babič A, Kovalenko S, Krivoruchenko M I, Šimkovic F *Phys. Rev. D* **98** 015003 (2018)
155. Bhupal Dev P S, Goswami S, Mitra M *Phys. Rev. D* **91** 113004 (2015)
156. de Salas P F et al. *Phys. Lett. B* **782** 633 (2018)
157. Šimkovic F et al. *Phys. Rev. C* **77** 045503 (2008)
158. Šimkovic F, Smetana A, Vogel P *Phys. Rev. C* **98** 064325 (2018)
159. Fang D-L, Faessler A, Šimkovic F *Phys. Rev. C* **97** 045503 (2018)
160. Mustonen M T, Engel J *Phys. Rev. C* **87** 064302 (2013)
161. Rath P K et al. *Phys. Rev. C* **88** 064322 (2013)
162. Vaquero N L, Rodríguez T R, Egido J L *Phys. Rev. Lett.* **111** 142501 (2013)
163. Yao J M et al. *Phys. Rev. C* **91** 024316 (2015)
164. Yao J M, Engel J *Phys. Rev. C* **94** 014306 (2016)
165. Cappuzzello F et al. *Eur. Phys. J. A* **54** 72 (2018)
166. Agodi C et al. (NUMEN Collab.) *Universe* **7** 72 (2021)
167. Lenske H et al. *Universe* **7** 98 (2021)
168. Šimkovic F et al. *Phys. Rev. C* **79** 055501 (2009)
169. Šimkovic F et al. *Phys. Rev. C* **83** 015502 (2011)
170. Caurier E et al. *Rev. Mod. Phys.* **77** 427 (2005)
171. Faessler A et al. *J. Phys. G* **35** 075104 (2008)
172. Barea J, Kotila J, Iachello F *Phys. Rev. C* **87** 014315 (2013)
173. Suhonen J, Civitarese O *Phys. Lett. B* **725** 153 (2013)
174. Deppisch F F, Suhonen J *Phys. Rev. C* **94** 055501 (2016)
175. Gysbers P et al. *Nat. Phys.* **15** 428 (2019)
176. Menéndez J, Gazit D, Schwenk A *Phys. Rev. Lett.* **107** 062501 (2011)
177. Engel J, Šimkovic F, Vogel P *Phys. Rev. C* **89** 064308 (2014)
178. Zinatulina D et al. *Phys. Rev. C* **99** 024327 (2019)
179. Jokiniemi L, Suhonen J *Phys. Rev. C* **100** 014619 (2019)
180. Šimkovic F, Dvornický R, Vogel P *Phys. Rev. C* **102** 034301 (2020)
181. Zinner N T, Langanke K, Vogel P *Phys. Rev. C* **74** 024326 (2006)
182. Kolbe E, Langanke K, Vogel P *Phys. Rev. C* **62** 055502 (2000)
183. Marketin T et al. *Phys. Rev. C* **79** 054323 (2009)
184. Elliott S R, Hahn A A, Moe M K *Phys. Rev. Lett.* **59** 2020 (1987)
185. Barabash A *Universe* **6** (10) 159 (2020)
186. Štefánik D, Šimkovic F, Faessler A *Phys. Rev. C* **91** 064311 (2015)
187. Rodin V A, Faessler A, Šimkovic F, Vogel P *Phys. Rev. C* **68** 044302 (2003)
188. Rodin V A, Faessler A, Šimkovic F, Vogel P *Nucl. Phys. A* **766** 107 (2006)
189. Rodin V A, Faessler A, Šimkovic F, Vogel P *Nucl. Phys. A* **793** 213 (2007) Erratum
190. Caurier E et al. *Phys. Rev. Lett.* **77** 1954 (1996)
191. Muto K, Bender E, Klapdor-Kleingrothaus H V *Z. Phys. A* **339** 435 (1991)
192. Deppisch F F, Graf L, Šimkovic F *Phys. Rev. Lett.* **125** 171801 (2020)
193. Deppisch F F et al. *Phys. Rev. D* **102** 051701 (2020)
194. Bolton P, Deppisch F F, Gráf L, Šimkovic F *Phys. Rev. D* **103** 055019 (2021)
195. Barabash A S et al. *Nucl. Phys. B* **783** 90 (2007)
196. Albert J B et al. (EXO-200 Collab.) *Phys. Rev. D* **93** 072001 (2016)
197. Azzolini O et al. *Phys. Rev. D* **100** 092002 (2019)
198. Nitescu O, Ghinescu S, Stoica S *J. Phys. G* **47** 055112 (2020)
199. Nitescu O V et al. *Phys. Rev. D* **103** L031701 (2021)
200. Arnold R et al. (NEMO Collab.) *Nucl. Phys. A* **765** 483 (2006)
201. Arnold R et al. *Eur. Phys. J. C* **79** 440 (2019)
202. Arnold R et al. (NEMO-3 Collab.) *Phys. Rev. Lett.* **119** 041801 (2017)
203. Šimkovic F, Domin P, Semenov S V *J. Phys. G* **27** 2233 (2001)
204. Domin P, Kovalenko S, Šimkovic F, Semenov S V *Nucl. Phys. A* **753** 337 (2005)
205. Arnold R et al. *Eur. Phys. J. C* **79** 440 (2019)
206. Azzolini O et al. *Phys. Rev. Lett.* **123** 262501 (2019)
207. Šimkovic F et al. *Phys. Rev. C* **97** 034315 (2018)
208. Gando A et al. (KamLAND-Zen Collab.) *Phys. Rev. Lett.* **122** 192501 (2019)